Biological activity and computational analysis of novel acrylonitrile derived benzazoles as potent antiproliferative agents for pancreatic adenocarcinoma with antioxidative properties

Anja Beč[1±], Leentje Persoons[2±], Dirk Daelemans[2], Kristina Starčević[3], Robert Vianello[4]* and Marijana Hranjec[1]*

[1]Department of Organic Chemistry, Faculty of Chemical Engineering and Technology, University of Zagreb, Marulićev trg 19, HR-10000 Zagreb, Croatia;

[2]KU Leuven Department of Microbiology, Immunology and Transplantation, Laboratory of Virology and Chemotherapy, Rega Institute, Leuven, Belgium;

[3]Department of Chemistry and Biochemistry, Faculty of Veterinary Medicine, University of Zagreb, Heinzelova 55, HR-10000 Zagreb, Croatia

[4]Laboratory for the computational design and synthesis of functional materials, Division of Organic Chemistry and Biochemistry, Ruđer Bošković Institute, Bijenička cesta 54, HR-10000 Zagreb, Croatia;

± These two authors have contributed equally to this.

Corresponding author: Dr. Marijana Hranjec, Full Prof., Department of Organic Chemistry, Faculty of Chemical Engineering and Technology, University of Zagreb, Marulićev trg 20, P.O. Box 177, HR-10000 Zagreb, Croatia, e-mail: mhranjec@fkit.hr; Dr. Robert Vianello, Laboratory for the computational design and synthesis of functional materials, Division of Organic Chemistry and Biochemistry, Ruđer Bošković Institute, Bijenička cesta 54, HR-10000 Zagreb, Croatia, e-mail: robert.vianello@irb.hr

Abstract

Continuing our research into the anticancer properties of acrylonitriles, we present a study involving the design, synthesis, computational analysis, and biological assessment of novel acrylonitriles derived from methoxy, hydroxy, and N-substituted benzazole. Our aim was to examine how varying the number of methoxy and hydroxy groups, as well as the N-substituents on the benzimidazole core, influences their biological activity.

The newly synthesized acrylonitriles exhibited strong and selective antiproliferative effects against the Capan-1 pancreatic adenocarcinoma cell line, with IC_{50} values ranging from 1.2 to 5.3 μM. Consequently, these compounds were further evaluated in three other pancreatic adenocarcinoma cell lines, while their impact on normal PBMC cells was also investigated to determine selectivity. Among these compounds, the monohydroxy-substituted benzimidazole derivative **27** emerged with the most profound and broad-spectrum anticancer antiproliferative activity being emerged as a promising lead candidate.

Moreover, a majority of the acrylonitriles in this series exhibited significant antioxidative activity, surpassing that of the reference molecule BHT, as demonstrated by the FRAP assay (ranging from 3200 to 5235 mmolFe^{2+}/mmolC). Computational analysis highlighted the prevalence of electron ionization in conferring antioxidant properties, with computed ionization energies correlating well with observed activities.

Key words: acrylonitriles, antioxidant activity, antiproliferative activity, benzimidazoles, benzothiazoles, pancreatic cancer

1. Introduction

Cancer remains a significant global health concern, with pancreatic cancer ranking as the seventh leading cause of cancer-related deaths.[1,2] Its aggressive nature, early metastasis, resistance to conventional chemotherapy, and poor patient prognosis contribute to its severity.[3,4] Among pancreatic cancers, pancreatic ductal adenocarcinoma (PDAC) stands out as one of the most prevalent and aggressive forms.[5] One of the major drawbacks in the treatment of pancreatic cancer is its resistance to chemotherapy. Researchers considered that the poor clinical outcomes may be attributed to the highly aggressive, metastatic and complex immunosuppressive tumor microenvironment of this disease. Therefore, the development of novel and effective therapeutic strategies is vital to improving treatments that are targeted. Over the past decade, significant research has been directed towards the development of immune checkpoint inhibitors and small molecule kinase inhibitors as potential pancreatic cancer treatments.[6,7,8,9]

In pancreatic cancer cells, there's a notable increase in reactive oxygen species (ROS) compared to normal cells.[10] Recent research has highlighted ROS as a potential target for novel therapeutic strategies in pancreatic cancer treatment.[11,12] These species play a crucial role in regulating cellular processes, including signaling, proliferation, survival, oxidative damage, and cell death. Their impact on cancer is dual, contingent on their intracellular concentration.[13–16]

Moderate ROS levels often activate cell survival pathways, aiding cancer cells in resisting detrimental effects. In early cancer stages, heightened ROS levels can initiate gene mutations and tumor growth, while increased concentrations may induce cell cycle arrest and cell death. In advanced stages, promoting ROS production might be considered beneficial.[17–19]

Antioxidants play a role in reducing oxidative DNA damage and gene mutations, potentially guarding against pancreatic cancer development.[20,21] Their biological effects are linked to scavenging free radicals and modulating cell signaling pathways.[22] To achieve this, they must regulate the cell cycle, inhibit tumor cell proliferation, induce apoptosis, decrease inflammation, and activate detoxification enzymes. Hence, strategies aimed at reducing ROS could be effective in preventing pancreatic cancer initiation.[23–26] Polyphenols have garnered significant attention for their potential chemo preventive mechanisms.[27,28] They possess diverse properties and biological effects, often acting as antioxidants due to the electron-donating phenolic groups within their structures.[29,30]

In our previous studies, our research teams disclosed the wide-ranging antioxidative and antiproliferative capabilities of diverse benzimidazole and benzothiazole derivatives.[31,32] These derivatives featured varying numbers of methoxy and hydroxy groups, and their biological characteristics were notably influenced by their chemical makeup, specifically the quantity and

arrangement of methoxy and hydroxy groups on the aromatic ring. [33,34] Additionally, acrylonitriles bearing a heteroaromatic core at the 2-position of the acrylonitrile structure, particularly 2,3-disubstituted acrylonitriles, have garnered significant attention owing to their diverse biological activities.

The acrylonitrile segment, characterized by high polarity and electron-withdrawing properties, possesses the ability to form hydrogen bonds with crucial amino acid residues in the active sites of diverse enzymes.[35,36,37,38,39] For instance, certain acrylonitrile compounds containing a benzotriazole[40] or indole[41] moiety have exhibited antiproliferative properties by engaging with tubulin at the colchicine-binding site, thereby disrupting tubulin polymerization. In our ongoing efforts to synthesize potent benzimidazole derivatives with significant antiproliferative effects, we developed novel N-substituted, benzimidazole-derived acrylonitriles aimed at potentially inhibiting tubulin polymerization. Specifically, compounds **I** and **II** featuring *N,N*-dimethyl amino and *N,N*-diethylamino substitutions (Figure 1) demonstrated growth inhibition across all tested cancer cell lines without adversely impacting normal cell viability. Their ability to interfere with tubulin polymerization was validated through in vitro experimentation and computational analysis. [42,43]

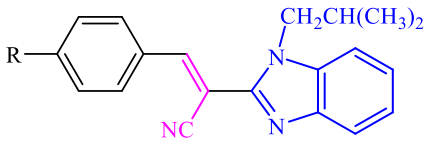

I R = *N*,*N*-$(CH_3)_2$
II R = *N*,*N*-$(CH_2CH_3)_2$

Figure 1. Benzimidazole derived acrylonitriles **I** and **II** as tubulin polymerization inhibitors

In this study, we expanded our research by designing and synthesizing new derivatives of benzazole acrylonitriles, encompassing benzimidazole or benzothiazole frameworks with methoxy and hydroxy group substitutions on the phenyl ring. Our primary goal was to examine how varying the quantity and placement of methoxy and hydroxy groups, along with the type of substituent introduced at the benzimidazole N atom, influences both antiproliferative and antioxidative properties. To delve deeper into the biological mechanism underlying these effects, additional experiments were conducted to establish any correlation between the antiproliferative activity and their ability to scavenge radicals. Furthermore, computational Density Functional Theory (DFT) analysis was employed to elucidate the chemical processes involved and identify the structural and electronic characteristics responsible for the observed antioxidant activities.

2. Results and discussion

2.1. Chemistry

The targeted benzimidazole derived acrylonitriles were synthesized via the experimental pathway shown in Scheme 1.

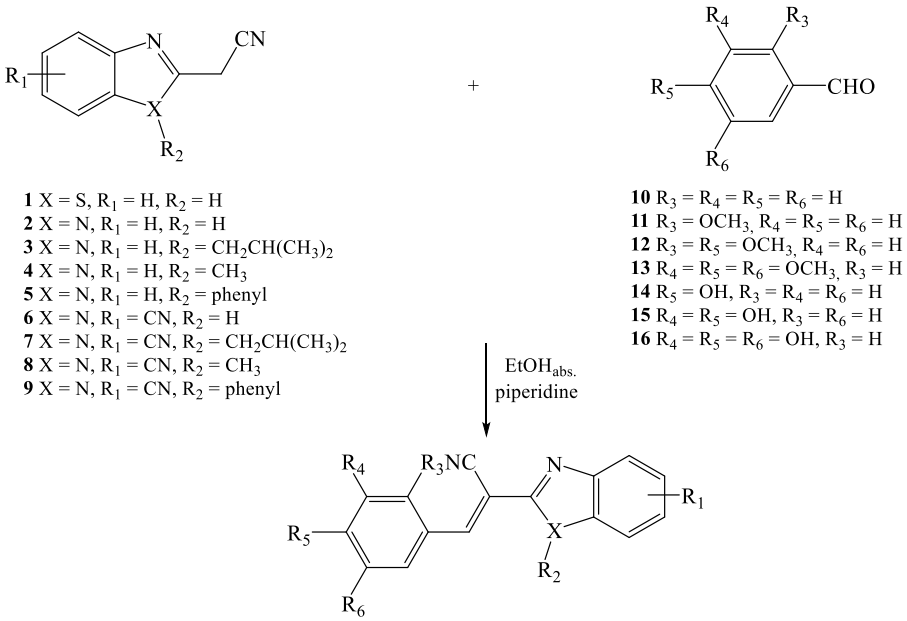

1 X = S, R_1 = H, R_2 = H
2 X = N, R_1 = H, R_2 = H
3 X = N, R_1 = H, R_2 = $CH_2CH(CH_3)_2$
4 X = N, R_1 = H, R_2 = CH_3
5 X = N, R_1 = H, R_2 = phenyl
6 X = N, R_1 = CN, R_2 = H
7 X = N, R_1 = CN, R_2 = $CH_2CH(CH_3)_2$
8 X = N, R_1 = CN, R_2 = CH_3
9 X = N, R_1 = CN, R_2 = phenyl

10 R_3 = R_4 = R_5 = R_6 = H
11 R_3 = OCH_3, R_4 = R_5 = R_6 = H
12 R_3 = R_5 = OCH_3, R_4 = R_6 = H
13 R_4 = R_5 = R_6 = OCH_3, R_3 = H
14 R_5 = OH, R_3 = R_4 = R_6 = H
15 R_4 = R_5 = OH, R_3 = R_6 = H
16 R_4 = R_5 = R_6 = OH, R_3 = H

17 X = S, R_1 = H, R_2 = H, R_3 = R_4 = R_5 = R_6 = H
18 X = S, R_1 = H, R_2 = H, R_3 = OCH_3, R_4 = R_5 = R_6 = H
19 X = S, R_1 = H, R_2 = H, R_3 = R_5 = OCH_3, R_4 = R_6 = H
20 X = S, R_1 = H, R_2 = H, R_4 = R_5 = R_6 = OCH_3, R_3 = H
21 X = S, R_1 = H, R_2 = H, R_5 = OH, R_3 = R_4 = R_6 = H
22 X = S, R_1 = H, R_2 = H, R_4 = R_5 = OH, R_3 = R_6 = H
23 X = S, R_1 = H, R_2 = H, R_4 = R_5 = R_6 = OH, R_3 = H
24 X = N, R_1 = H, R_2 = H, R_5 = OH, R_3 = R_4 = R_6 = H
25 X = N, R_1 = H, R_2 = H, R_4 = R_5 = OH, R_3 = R_6 = H
26 X = N, R_1 = H, R_2 = H, R_4 = R_5 = R_6 = OH, R_3 = H
27 X = N, R_1 = CN, R_2 = H, R_5 = OH, R_3 = R_4 = R_6 = H
28 X = N, R_1 = CN, R_2 = H, R_4 = R_5 = OH, R_3 = R_6 = H
29 X = N, R_1 = CN, R_2 = H, R_4 = R_5 = R_6 = OH, R_3 = H
30 X = N, R_1 = H, R_2 = $CH_2CH(CH_3)_2$, R_5 = OH, R_3 = R_4 = R_6 = H
31 X = N, R_1 = H, R_2 = $CH_2CH(CH_3)_2$, R_4 = R_5 = OH, R_3 = R_6 = H
32 X = N, R_1 = H, R_2 = $CH_2CH(CH_3)_2$, R_4 = R_5 = R_6 = OH, R_3 = H

33 X = N, R_1 = CN, R_2 = $CH_2CH(CH_3)_2$, R_5 = OH, R_3 = R_4 = R_6 = H
34 X = N, R_1 = CN, R_2 = $CH_2CH(CH_3)_2$, R_4 = R_5 = OH, R_3 = R_6 = H
35 X = N, R_1 = CN, R_2 = $CH_2CH(CH_3)_2$, R_4 = R_5 = R_6 = OH, R_3 = H
36 X = N, R_1 = H, R_2 = CH_3, R_5 = OH, R_3 = R_4 = R_6 = H
37 X = N, R_1 = H, R_2 = CH_3, R_4 = R_5 = OH, R_3 = R_6 = H
38 X = N, R_1 = H, R_2 = CH_3, R_4 = R_5 = R_6 = OH, R_3 = H
39 X = N, R_1 = CN, R = CH_3, R_4 = OH, R_2 = R_3 = R_5 = H
40 X = N, R_1 = CN, R = CH_3, R_4 = R_5 = OH, R_3 = R_6 = H
41 X = N, R_1 = CN, R = CH_3, R_4 = R_5 = R_6 = OH, R_3 = H
42 X = N, R_1 = H, R_2 = phenyl, R_5 = OH, R_3 = R_4 = R_6 = H
43 X = N, R_1 = H, R_2 = phenyl, R_4 = R_5 = OH, R_3 = R_6 = H
44 X = N, R_1 = H, R_2 = phenyl, R_4 = R_5 = R_6 = OH, R_3 = H
45 X = N, R_1 = CN, R_2 = phenyl, R_5 = OH, R_3 = R_4 = R_6 = H
46 X = N, R_1 = CN, R_2 = phenyl, R_4 = R_5 = OH, R_3 = R_6 = H
47 X = N, R_1 = CN, R_2 = phenyl, R_4 = R_5 = R_6 = OH, R_3 = H

Scheme 1. Synthesis of benzazole derived acrylonitriles **17–47**

The key precursors required for synthesizing the final acrylonitriles derived from benzimidazole specifically, the N-substituted 2-cyanomethylbenzimidazoles **2–9** were prepared following established procedures outlined in previously published works, yielding similar reaction yields as reported.[38,39] The targeted benzazole-derived acrylonitriles **17–47** were synthesized via the Knoevenagel condensation reaction. This involved utilizing commercially available 2-benzothiazoleacetonitrile **1** and the prepared N-substituted 2-cyanomethylbenzimidazoles **2–9**, in conjunction with benzaldehyde **10**, methoxy-substituted **11–13**, and hydroxy-substituted **14–16** aromatic aldehydes. The reactions were carried out in absolute ethanol using drops of piperidine as a mild base catalyst.

This method presents a direct approach for synthesizing acrylonitriles, capitalizing on the acidic nature of the methylene group present in the precursors. This acidity is activated by both the cyano group and the benzazole structure. Despite the possibility of obtaining two geometric isomers from the Knoevenagel condensation, only E-isomers were exclusively obtained in this new series. The desired acrylonitrile derivatives **17–47** were acquired with varying yields ranging from 16% to 88%. Purification was carried out through recrystallization from ethanol or by column chromatography. Among these derivatives, the lowest overall yields were observed in the synthesis of compounds **32** (20%) and **34** (25%), both featuring an isobutyl chain on the benzimidazole nitrogen, along with two or three hydroxy groups on the phenyl ring. Similarly, derivative **43** (16%), substituted with a phenyl ring and two hydroxy groups, exhibited lower yields, likely attributed to steric hindrance caused by the size of the substituents on the benzimidazole ring. The identification of the isolated acrylonitrile structures relied on 1H and 13C NMR spectroscopy as well as elemental analysis. Structural elucidation involved analyzing chemical shifts in both spectra and H-H coupling constant values in the 1H spectra. In the 1H NMR spectra, a singlet signal was observed around 7.47–8.56 ppm, attributed to the vinylic proton of the acrylonitrile group across all compounds. The proton peak corresponding to the OH group of hydroxy groups manifested as a broad singlet signal within the range of 10.68–3.59 ppm. In some spectra, not every peak was observable due to hydrogen bonding and proton exchange with deuterium atoms from the solvent.

2.2. Biological evaluation

2.2.1. Effects of novel acrylonitrile derived benzazoles on cancer cell line proliferation

All newly prepared compounds were tested for their *in vitro* antiproliferative activity against a panel of various cancer cell lines. For the initial antitumoral evaluation, eight human cancer cell lines from different cancer types were used (Capan-1–pancreatic adenocarcinoma; HCT-116–colorectal carcinoma; LN229–glioblastoma; NCI-H460–lung carcinoma; DND-41–acute lymphoblastic leukemia; HL-60–acute myeloid leukemia; K-562–chronic myeloid leukemia; Z-138–non-Hodgkin lymphoma). The known antineoplastic agent etoposide is included for comparison. An overview of the results is shown in Figure 2, left panel.

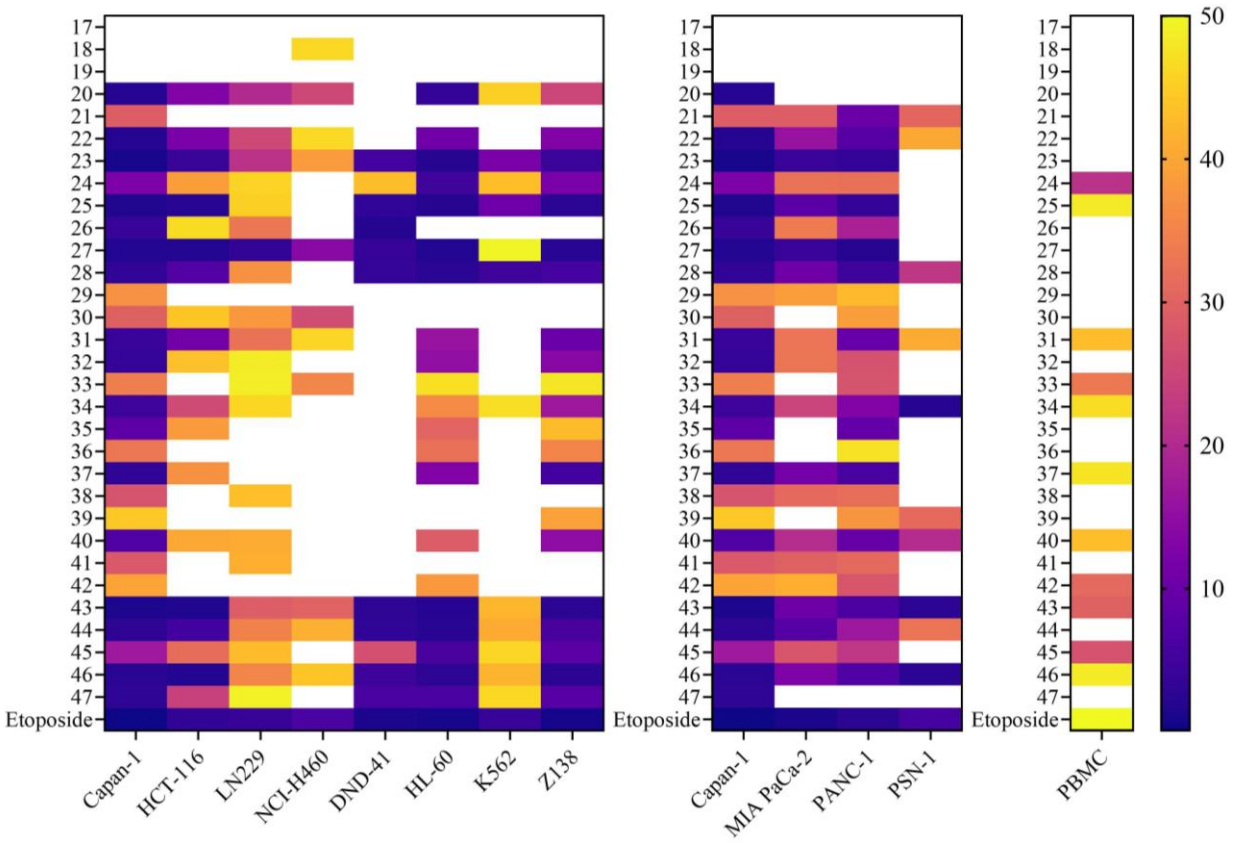

Figure 2. Heat map of cell-growth inhibition induced by the indicated acrylonitrile derived benzazoles in the various cell lines. Left panel depicts results in diverse cancer cell types, middle panel represents results in four pancreatic adenocarcinoma cell lines and right panel displays the effects on normal PBMC. Cell responses were visualized as a heat map, where IC50 values (μM) are plotted for each compound. Dark purple indicates potent inhibition of cell growth (low IC_{50} values), whereas yellow to white indicates little to no effect on cell viability (high IC_{50} values).

In the initial antitumoral evaluation, compounds **20**, **22**, **23**, **25**, **26**, **27**, **28**, **43**, **44**, **46** and **47** demonstrated significant antiproliferative activity ($IC_{50} \leq 3$ μM). Benzothiazole **20**, **22** and **23** and benzimidazole derivatives **25–28**, **31**, **32**, **34**, **37**, **40**, **43–44**, **46–47** showed selective inhibitory effects against the pancreatic adenocarcinoma cell line (Capan-1) in low micromolar concentrations. Among the benzothiazole-substituted acrylonitrile derivatives, in general, the hydroxy-substituted derivatives showed better activity when compared to the methoxy-substituted derivatives. Trihydroxy-substituted derivative **23** showed significant antiproliferative activity against the pancreatic cancer (Capan-1) and the acute myeloid leukemia (HL-60) cell lines.

Among all tested derivatives, the most pronounced broad anticancer activity (Capan-1 (IC_{50} = 1.1 μM), HCT-116 (IC_{50} = 1.7 μM), LN229 (IC_{50} = 3.4 μM) and HL-60 (IC_{50} = 1.7 μM)) was noted for the monohydroxy-substituted benzimidazole derivative **27**, lacking a substituent on the benzimidazole nitrogen but with a cyano group at the C-5(6) position of the benzimidazole. Comparing the inhibitory activity of di- and trihydroxy-substituted benzimidazole derivatives **25** and **26**, derivative **25** showed a better antitumoral profile, from which it can be concluded that the anticancer activity is influenced by the number and position of the hydroxy groups on the phenyl ring. The N-phenyl substituted benzimidazole derivatives **43** and **46** with two hydroxy groups showed strong inhibitory activity against both the pancreatic cancer cell line Capan-1 (**43** IC_{50} = 1.5 μM, **46** IC_{50} = 1.7 μM) and the colorectal carcinoma cell line HCT-116 (**43** IC_{50} = 1 .5 μM, **46** IC_{50} = 1.7 μM). Overall, derivative **43** showed better activity than the cyano-substituted analogue **46** indicating that the cyano group on the benzimidazole ring is not crucial for activity. By introducing substituents on the N atom of the benzimidazole nucleus, the antiproliferative activity decreases, and the substituents on the benzimidazole nitrogen decreased the activity in the following order: isobutyl > methyl > phenyl > H. Considering that benzothiazole derivatives **20**, **22** and **23** and benzimidazole **25–28**, **31**, **32**, **34**, **37**, **40**, **43–44**, **46–47** showed marked inhibitory action against the Capan-1 pancreatic adenocarcinoma cell line, the antiproliferative activity against three additional pancreatic adenocarcinoma cell lines (MIA PaCa-2, PANC-1 and PSN-1) was evaluated (Figure 2, middle panel).

The monohydroxy-substituted derivative **27** without a substituent on the benzimidazole nitrogen and a cyano group at position C-5(6) on the benzimidazole displayed pronounced antiproliferative effects against three different pancreatic adenocarcinoma cell lines (Capan-1, MIA PaCa-2 and PANC-1, IC_{50} = 2.0–4.1 μM)against. Likewise, the trihydroxy-substituted benzothiazole derivative **23** showed significant antiproliferative activity against the same three pancreatic adenocarcinomas with potent selective activity against Capan-1 (IC_{50} = 0.8 μM). Derivatives **34**, **43** and **46** (IC_{50} = 1.9–2.7 μM) showed general anti pancreatic cancer activity, including against the PSN-1 cell line. Besides determining the anticancer activities of all acrylonitrile derived benzazoles, their effects on the viability of normal cells were evaluated. In order to establish whether the observed antiproliferative activity is selective towards cancer cells, the cytotoxicity against normal peripheral blood mononuclear cells (PBMC) were measured (Figure 1, right panel).

Overall, minimal impact on PBMC viability was observed, with all IC_{50} values above 20 μM, indicating promising selectivity for anticancer effects while sparing normal cells.

2.2.2. Most potent acrylonitrile derived benzazoles inhibit the growth of pancreatic adenocarcinoma spheroids

In general, *in vitro* anticancer screening is based on cytotoxicity assays using cancer cell lines grown as two-dimensional (2D) cultures. This straight forward approach evidently has numerous strengths, making it a logic first tool for identifying promising new anticancer agents, but cytotoxicity screens based solely on 2D cultures also have important limitations. In particular, conventional 2D cancer cell cultures are not capable of mimicking the complex heterogeneity of clinical tumors. The three-dimensional (3D) growth of cancer cell lines is regarded as a more representative model for *in vitro* drug testing, displaying several *in vivo* characteristics of tumors. Solid tumor spheroids have emerged as a pivotal tool in evaluating the anticancer properties of novel derivatives due to their ability to closely mimic *in vivo* tumor architecture and physiology, surpassing traditional 2D monolayer cultures. Particularly, the glucose metabolism exhibited in 3D spheroids reflects the *in vivo* tumor metabolic conditions more accurately, underscoring the necessity of utilizing such models for investigating drugs targeting tumor metabolism.[44] By mirroring features like drug resistance mechanisms, gene expression patterns, and physiological responses, spheroids offer a more predictive environment for assessing the effectiveness of anticancer drugs compared to 2D cultures or animal models. The complex and dynamic nature of the tumor microenvironment (TME), comprising diverse cellular and non-cellular components, underscores the importance of utilizing 3D cell spheroids to better understand tumor biology and predict therapeutic outcomes.[45] Consequently, the shift towards 3D cell cultures is essential for accurately assessing therapeutic toxicity and efficacy by providing a more realistic representation of the TME, including physical and mechanical properties, oxygen, pH and nutrient gradients, and drug transport.[46] Therefore, the effects of the most potent acrylonitrile derived benzazoles on the growth of pancreatic adenocarcinoma cells in 3D culture were investigated.

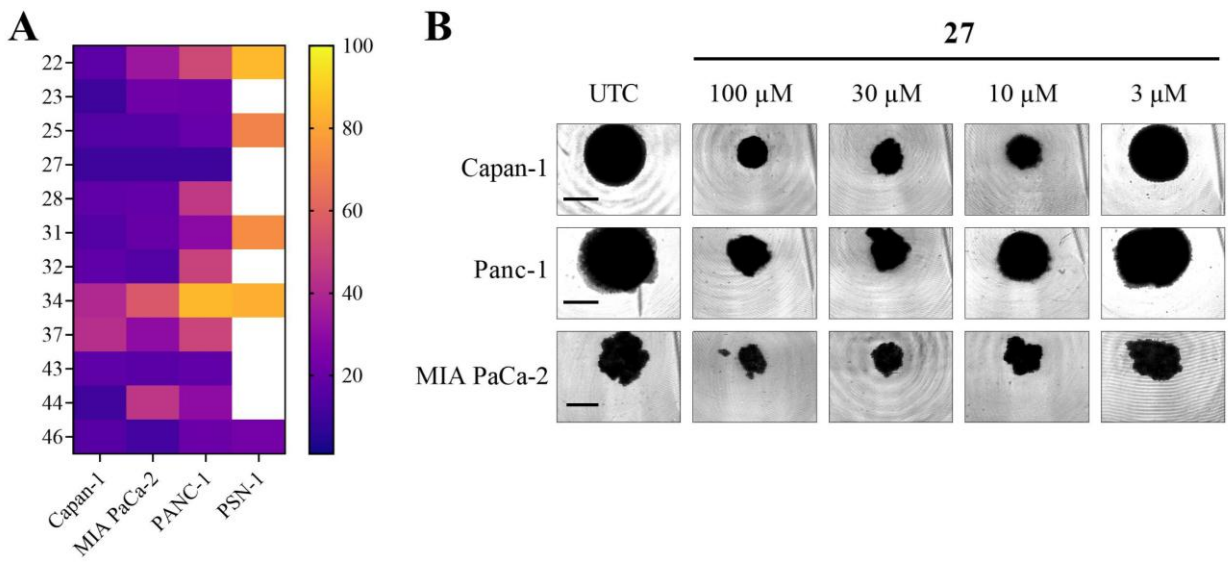

Figure 3. Selection of benzazoles inhibits the growth of pancreatic adenocarcinoma spheroids. (**A**) Heatmap representation of the IC_{50} values (µM) in 3D cultures of four pancreatic adenocarcinoma cell lines in the presence of the indicated compounds. (**B**) The growth of pancreatic tumor spheroids was dose dependently prevented by the addition of derivative **27** after spheroid formation. UTC, untreated control. Scale bars, 500 µm.

A selection of the most potent derivatives was further evaluated in multicellular tumor spheroid assays of the same four different pancreatic adenocarcinoma cell lines that were used for the initial 2D cytotoxicity screen.

Treatment of 3D spheroid cultures with the synthesized benzazoles caused visible changes in the morphology and size of the obtained spheroids in three of these cell lines (Capan-1, MIA PaCa-2 and PANC-1), whereas only subtle inhibitory effects were noted in PSN-1 spheroids. All selected benzazoles dose dependently inhibited the growth of Capan-1, MIA PaCa-2 and PANC-1 spheroids, and the obtained IC_{50} values are depicted in Figure 3 (left panel). Out of this selection, derivative **27** proved most potent, inhibiting the growth of Capan-1, MIA PaCa-2 and PANC-1 spheroids with IC_{50} values <10µM. Representative images of Capan-1, MIA PaCa-2 and PANC-1 spheroids after 10 days of treatment with derivative **27** and untreated controls (UTC) are shown in Figure 3 (right panel).

2.2.3. Derivative 27 induces G2/M cell cycle arrest and apoptosis in pancreatic adenocarcinoma cells

To characterize derivative **27** as a novel inhibitor of pancreatic adenocarcinoma cells, the effect of this compound on the cell cycle distribution of Capan-1 cancer cells was examined (Figure 4 A).

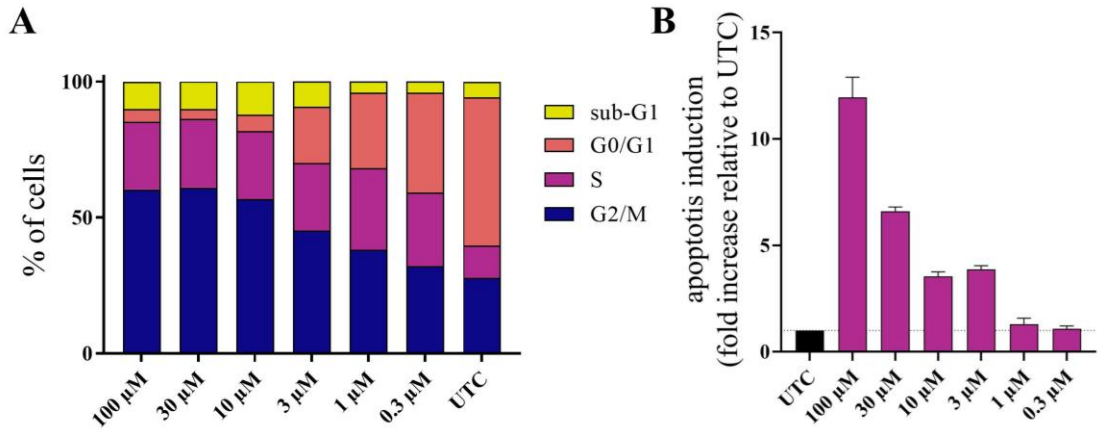

Figure 4. Derivative **27** induces G2/M cell cycle arrest and apoptosis in Capan-1 cells treated with indicated concentrations of AOH-011 for 24 h. (**A**) Following DAPI staining, the distribution of cell cycle was assessed by high content analysis, and the percentage of cells in each phase was determined. (**B**) Cells were stained with CellEvent TM Caspase-3/7 Green Reagent and Hoechst 33342, and apoptosis induction was measured by high content analysis

DAPI staining was conducted to assess the cell cycle progression subsequent to treatment with varying doses of compound 27. The findings suggest a notable elevation in the proportion of Capan-1 cells in the G2/M phase upon exposure to compound 27 compared to untreated control cells (UTC). Additionally, comprehensive analysis revealed that treatment with derivative 27 significantly and in a dose-dependent manner triggered apoptosis in Capan-1 cells (Figure 4 B).

2.2.4. Derivative 27 reduces clonogenic survival of pancreatic adenocarcinoma cells

The effect of lead compound **27** on the capacity of pancreatic adenocarcinoma cells to form colonies was examined. As shown in Figure 5, the number of colonies was markedly reduced in the treated wells compared to the controls. For Capan-1, the number of formed colonies was significantly reduced, even at very low concentrations (Figure 5, top panels). Colony formation of Panc-1 cells was also inhibited in a dose dependent manner, with a smaller number of colonies compared to the untreated controls for all tested concentrations (Figure 5, bottom panels).

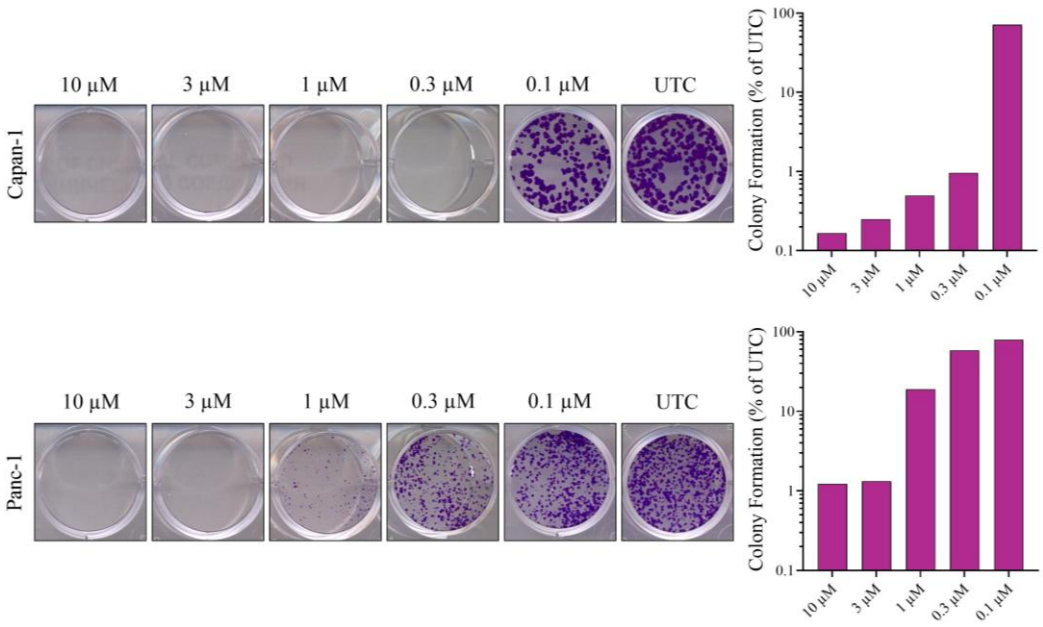

Figure 5. 27 treatment decreases the colony formation ability of pancreatic adenocarcinoma cells. **27** was administered at different concentrations to Capan-1 (upper panel), and Panc-1 (bottom panel). Representative images are shown, and the quantification of the number of clones is shown in the right panel as bar graphs. Cells were visualized with crystal violet and amount of colonies was normalized to the number of colonies in the untreated wells.

2.2.5. Antioxidant and hemolysis protective effect of novel acrylonitrile derived benzazoles

To explore the general *in vitro* antioxidant activity of the benzazole acrylonitrile derivatives, the reducing power of the stable radical 1,1-diphenyl-picrylhydrazyl (DPPH), the free radical scavenging ability by using the radical cation 2,2-azinobis-(3-ethylbenzthiazoline-6-sulphonic acid (ABTS) and the ferric reducing/antioxidant power (FRAP) were evaluated. The evaluation was conducted by *in vitro* spectrometric methods, and. the well-known antioxidant butylated hydroxytoluene (BHT) was included as a positive control. The results are expressed as IC_{50} values and are presented in Table 1.

The results of these antioxidant activity tests showed that hydroxy groups play an important role in improving the activity of these compounds, which is in line with previous research by our group. Weak antioxidant activity of methoxy-substituted benzothiazole derivatives **17**–**21** was obtained by all methods used. The di- and trihydroxy-substituted derivatives **22** and **23** proved to be the most potent antioxidative benzothiazoles. All benzimidazole derivatives showed exceptional antioxidant activity in the FRAP assay, reducing ferric tripyridyl triazine complex (TPTZ) to ferrous (Fe^{2+}) form, with superior activity when compared to the positive control BHT.

The overall best reducing ability was shown by derivative **28**, lacking a substituent on the N-atom of the benzimidazole and bearing two hydroxy groups. Derivatives with methyl and phenyl groups generally showed improved activity compared to derivatives with an isobutyl substituent on the N-atom of the benzimidazole nucleus.

Table 1. *In vitro* antioxidative activities of compounds **17**–**47**

Cpd.	FRAP/mmolFe^{2+}/mg cpd	ABTS/µM	DPPH/µM
17	101.48±1.15	-	-
18	112.41±1.67	-	-
19	137.26±0.95	-	-
20	113.24±0.62	-	-
21	25.04±0.82	5910±775	-
22	3890.09±13.49	69.6±7.4	63.2±6.71
23	4071.81±14.83	55.1±0.0424	65.6±6.59
24	31.93±2.06	9096±849	-
25	4536.19±41.30	71.2±0.071	61.6±6.24
26	4563.50±27.68	55.6±0.184	70.3±6.91
27	36.20±5.06	3940±369	-
28	5235.72±80.70	59.0±0.445	46.7±4.93
29	3628.81±12.85	56.3±0.12	73.4±7.43
30	257.35±18.99	1220±12.2	2960±264.5
31	3677.50±14.40	75.1±7.7	78.4±7.95
32	3277.26±26.26	59.5±6.08	80.2±8.1
33	26.70±2.57	1753.0±91.7	-
34	2205.98±13.49	105.0±10.6	163.0±16.6
35	3242.82±47.85	69.2±6.77	94.7±8.84
36	49.03±2.50	244.0±7.46	-
37	4018.36±17.93	62.8±0.017	73.6±7.42
38	3761.83±23.18	51.5±0133.0	75.6±7.76
39	22.90±1.09	1960.0±223.0	-
40	3537.36±14.83	62.9±3.68	86.4±9.05
41	3730.95±23.18	5.58±5.5	77.2±7.5
42	48.08±3.97	-	-
43	3565.86±28.80	6.9±6.88	99.3±0.1
44	3511.23±24.94	60.5±5.95	82.8±8.32
45	24.33±1.09	-	-
46	3382.96±21.67	70.9±7.19	93.1±932
47	3287.95±37.43	59.9±6.06	85.3±7.73
BHT	2089.34±55.98	23.1±1.2	25.0±4.2

According to the ABTS method, derivatives **41** and **43** with methyl and phenyl substituents and two hydroxy groups showed superior activity compared to the positive control. All tested derivatives showed little or no ability to reduce DPPH radicals. Taking into account all the results of the antioxidant evaluation, derivatives with two hydroxy groups generally showed an improved ability to deactivate radicals compared to derivatives with three hydroxy groups. The position of the hydroxy groups on the phenyl ring of the acrylonitrile appeared to have a greater influence on the antioxidant power than the number of these groups. The presence of hydroxy groups in the ortho-position gives greater stability to the phenoxy radical, which is formed by the reaction of antioxidants and radicals. Additionally, hydrogen peroxide (H2O2)-induced hemolysis of erythrocytes is a commonly used biological model for antioxidant activity evaluation.

To investigate the possible correlation between antioxidant and antiproliferative activity, the derivatives with promising anticancer activity (**22**, **23**, **25**, **27**, **28**, **31**, **32**, **34**, **37**, **40**, **43**, **44** and **46**) were subjected to a red blood cell hemolytic assay (Figure 6).

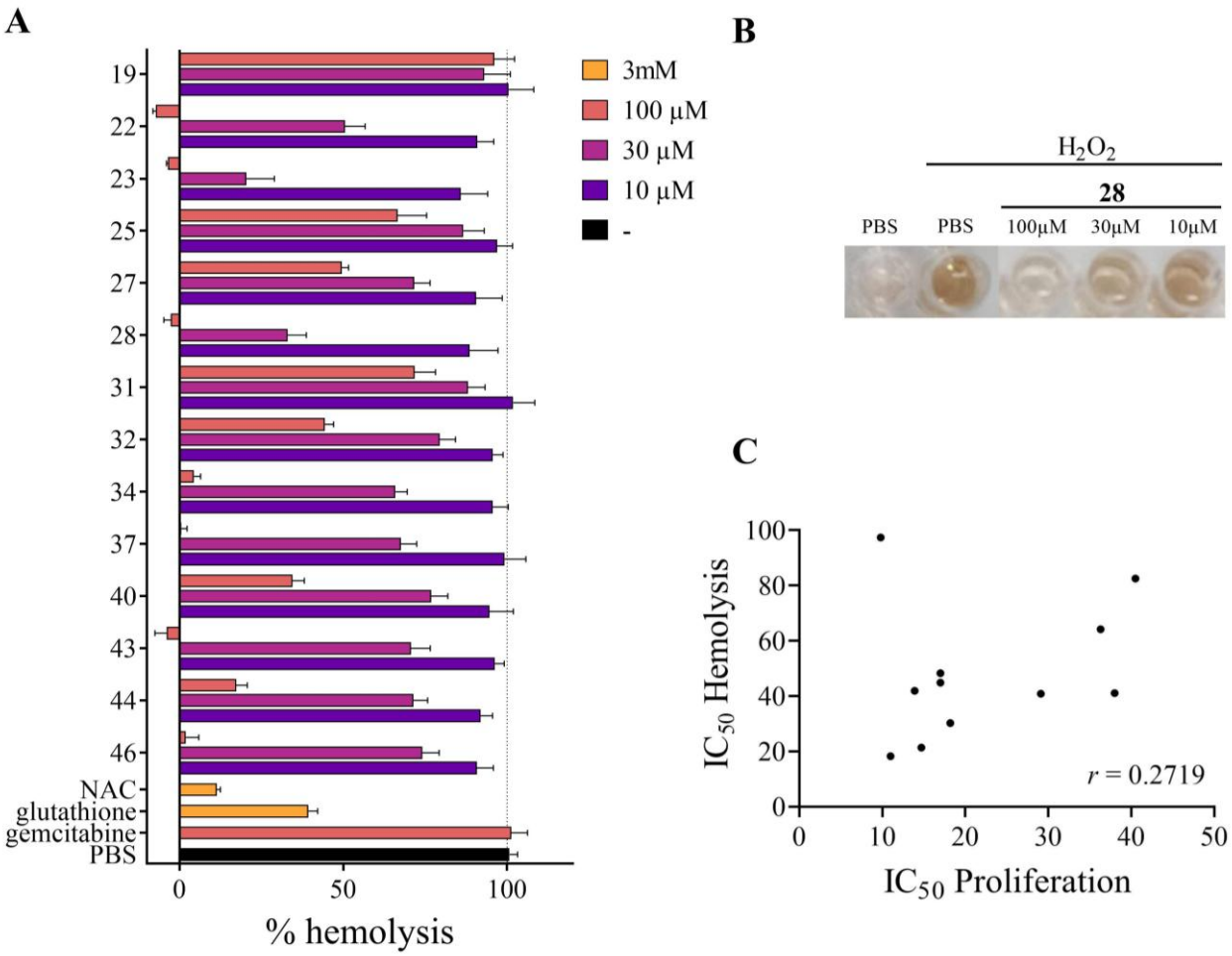

Figure 6. Protective effects of acrylonitriles on H_2O_2-induced erythrocyte hemolysis. (**A**) Erythrocytes were pretreated with different concentrations (100 - 30 - 10 μM) of the test compounds for 15 minutes prior to H_2O_2 treatment for 2 hours. The relative hemolysis was assessed in comparison with the hemolysis in the H_2O_2 treated negative control (PBS), which was set as 100 %. (**B**) A visual representation of the dose dependent antioxidant activity of **28**. (**C**) Low degree of correlation between anticancer activity (IC_{50} proliferation) and antioxidative activity (IC_{50} hemolysis).

N-acetyl-L-cysteine (NAC) and glutathione were included as positive controls, and antitumor drug gemcitabine and phosphate buffer (PBS) as negative controls. After the addition of hydrogen peroxide, which causes lipid peroxidation of the erythrocyte membrane, the level of hemolysis was measured spectrophotometrically, and the obtained results were compared with the control samples (PBS) in which maximal hemolysis occurs (100% hemolysis). For most derivatives, a dose dependent protective effect was noted. According to the obtained results increasing the concentration of the compound decreases the percentage of erythrocyte hemolysis.

Regression analysis indicated a very low degree of correlation between the measured antiproliferative and antioxidant activity ($r = 0.2719$, Figure 6C). It appears that the antioxidant activity of the synthesized acrylonitrile derivatives is not significantly associated with their antiproliferative activity. Consequently, further experiments are necessary to uncover the underlying mechanism of action regarding their anticancer effects.

Considering the collective biological findings, it is evident that several compounds exhibited potent antiproliferative activity against a range of pancreatic adenocarcinoma cells while demonstrating non-toxic effects on normal cells. Additionally, the majority of the newly synthesized derivatives displayed notably superior antioxidative potential. However, it appears that this antioxidative potential does not correlate with their anticancer activity. Through structure-activity analysis, it is apparent that the biological activity of the novel benzazole derived acrylonitriles is strongly influenced by the number of hydroxy groups and the type of substituent positioned at the benzimidazole N atom (Figure 7). Notably, the benzimidazoles displayed significantly higher biological activity compared to the benzothiazole analogues.

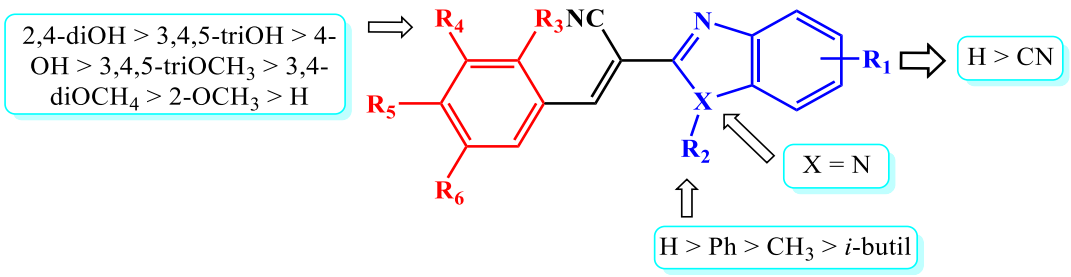

Figure 7. SAR analysis for benzazole derived acrylonitriles based on the antiproliferative and antioxidative activity

2.3. Computational analysis

Computational analysis was utilized to identify chemical processes governing the radical scavenging ability of investigated derivatives, and interpret the high antioxidant capacity of system **28**. For that purpose, we have calculated electron ionization energies (IEs) and hydrogen atom/proton release capacity of a selected number of systems, together with several model compounds in ethanol (Table 2), in order to provide enough structural and electronic features to help us in rationalizing measured data. In doing so, we have considered all systems as neutral unionized compounds based on acid/base constants for reference analogues found in the literature. Namely, since the ethanol autoproteolysis constant is 16.8,[47] the measured pK_a values of phenol (14.3), *o*-hydroxyphenol (16.2), *o*,*m*-dihydroxyphenol (14.6) and benzimidazole (6.7)[48] in that solvent indicate that all acid/base sites will remain unionized under experimental conditions.

Our analysis focuses on computed e^-/H$^\bullet$/H^+ releasing abilities that are placed in the context of experimentally employed assays. Specifically, when FRAP is used, it is obvious that the radical scavenging ability relies on the electron-donating SET mechanism that reduces a ferric Fe(III) complex into an ferrous Fe(II) analogue, for which IE values are crucial. In the other two assays, $ABTS^{\bullet+}$ and DPPH$^\bullet$, all three studied mechanisms are formally possible, yet our preceding work[49] demonstrated that the SET mechanism dominates in determining the antioxidant capacity in these two assays as well, with some relevance of the HAT mechanism for DPPH$^\bullet$, in line with similar reports in the literature.[50]

Table 2. Ionization energies IE, H• abstraction energies $\Delta G_R(H^•)$ and deprotonation energies $\Delta G_R(H^+)$ in ethanol calculated by the (SMD)/B3LYP/6–31+G(d) model (in kcal mol^{-1}).

System	Structure	IE	H• Abstraction		H+ Abstraction	
			Site	$\Delta G_R(H^•)$	Site	$\Delta G_R(H^+)$
17	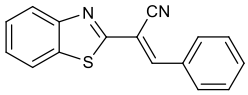	136.6	acrylo C–H	93.9	acrylo C–H	183.8
m1	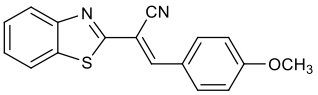	129.3	p-OCH_3	89.9	acrylo C–H	187.2
21	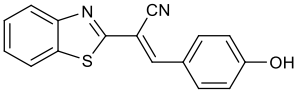	130.0	*p*-OH	70.1	*p*-OH	141.5
m2	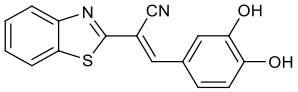	129.5	*p*-OH	65.9	*p*-OH	139.5
23	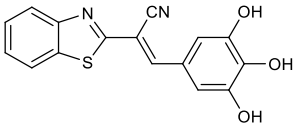	130.1	*p*-OH	62.2	*p*-OH	136.7
m3	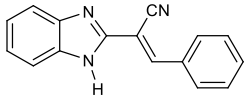	131.2	N–H	83.3	N–H	152.4
24	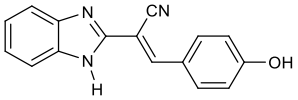	127.1	*p*-OH	70.6	*p*-OH	144.0
36	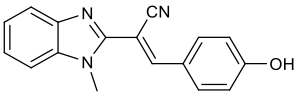	127.2	*p*-OH	70.9	*p*-OH	144.7
30	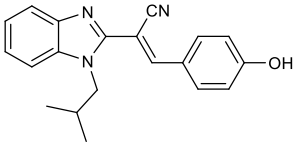	127.6	*p*-OH	71.1	*p*-OH	144.3
42	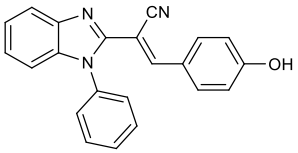	127.8	*p*-OH	71.4	*p*-OH	144.7
27	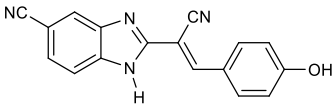	131.6	*p*-OH	72.3	*p*-OH	143.5
28	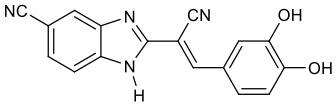	130.2	*p*-OH	66.3	*p*-OH	140.2
29	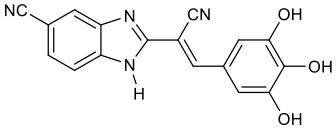	130.4	*p*-OH	62.2	*p*-OH	137.6

One thing that is immediately obvious from Table 4 is the fact that deprotonation energies are thermodynamically least favorable among all three processes, as they all exceed 136.7 kcal mol^{-1} calculated for **23**, where it pertains to the proton detachment from the *p*-OH group. With this, all $\Delta G_R(H^+)$ values are higher than any energy required for the electron ionization and the H$^\bullet$ abstraction in particular. This leads us to conclude that antioxidant activities measured in this work do not rely on the system deprotonation as the dominant radical scavenging mechanism. This is further supported by our calculations showing that the free energy gain to attach the proton to, for example, DPPH$^\bullet$ is –122.5 kcal mol^{-1}, thus being significantly lower than the required deprotonation energies. This leaves the thermodynamic misbalance among acid/base sites, and renders such a proton transfer unlikely.

As mentioned, the ability of investigated molecules to undergo electron ionization appears crucial in determining their antioxidant features, while their tendency to liberate the hydrogen atoms (H$^\bullet$) bears only a moderate relevance for the DPPH$^\bullet$ assay. The reason for that is the fact that both ABTS$^{\bullet+}$ and DPPH$^\bullet$ assays are related with electron affinities around 125 kcal mol^{-1},[42] which underlines a thermodynamic feasibility to accept an electron from all systems examined here (Table 4). In contrast, their exergonic energies to accept the hydrogen atom are –36.6 kcal mol^{-1} for ABTS$^{\bullet+}$ and –66.7 kcal mol^{-1} for DPPH$^\bullet$,[45] which validates some relevance of the H$^\bullet$ transfer process for the latter, but not for the former assay.

With this in mind, we will start the analysis with the parent benzothiazole **17**, whose electron ionization is associated with a high IE = 136.6 kcal mol^{-1} and also a very high $\Delta G_R(H^\bullet)$ = 93.9 kcal mol^{-1} that corresponds to the homolytic cleavage of the acrylic C–H bond. This justifies why **17** appears as a very poor antioxidant in all three assays. Still, its tendency to lose an electron can be improved by attaching the electron-donating group on the phenyl ring, which compensates the loss in the electron density following the ionization, thus stabilizes the formed radical cation through resonance and lowers IE values.

The methoxy group in the model system **m1** is relatively successful in this respect, as the calculated IE drops by 7.3 kcal mol^{-1} to IE = 129.3 kcal mol^{-1}, while it additionally sets up a better H$^\bullet$-donating group within its methoxy unit that reduces $\Delta G_R(H^\bullet)$ by 4.0 kcal mol^{-1} down to $\Delta G_R(H^\bullet)$ = 89.9 kcal mol^{-1}. The latter ties in with a general trend that saturated C(sp^3)–H groups typically require less energy for the homolytic bond cleavage over their unsaturated C(sp^2)–H and C(sp)–H analogues. Alternatively, the –OH group is somewhat less potent electron-donor than –OMe, which associates **21** with higher IE value over **m1** by 0.7 kcal mol^{-1}, which nicely justifies its lower FRAP activity over **17**. Yet, the hydroxy moiety introduces a very reactive center with a high tendency to undergo the homolytic O–H cleavage.

This is evident in its low $\Delta G_R(H^\bullet)$ = 70.1 kcal mol^{-1}, being reduced by as much 23.8 kcal mol^{-1} from **17**. Unfortunately, this is not confirmed by experiments as both ABTS and DPPH measurements for **17** could not have been recorded (Table 3), likely due to high C–H cleavage demands or even its kinetic hindrance. Nevertheless, the extension of this strategy leads to di- and trihydroxy derivatives **m2** and **23**, which confirm the preceding arguments. Namely, additional –OH groups only moderately affect IE values, especially since they are placed in less active *meta*-positions,[42] yet their ability to provide the stabilizing effect by forming the O–H···O$^\bullet$···H–O hydrogen bonding with the radical center following the H$^\bullet$ release, improves $\Delta G_R(H^\bullet)$ values and antioxidant features, in line with our earlier results on similar systems.[28,38,39,42] This makes **23** the most potent benzothiazole antioxidant probed computationally, tying in with experiments (Table 2). According to our calculations, benzimidazole offers a more promising skeleton for the design of potent antioxidants over benzothiazole, since its IE value is by 7.9 kcal mol^{-1} lower and assumes IE = 138.4 kcal mol^{-1} (146.3 kcal mol^{-1} in benzothiazole), while it also comes with a modest, yet much better tendency to liberate the H$^\bullet$ radical, $\Delta G_R(H^\bullet)$ = 89.3 kcal mol^{-1}, which is not matched by benzothiazole. Thus, it comes as a no surprise that **m3** turns as a better antioxidant over **17** in both aspects, with an additionally improvement in the N–H homolytic bond energy over parent benzimidazole, being lowered by 6.0 kcal mol^{-1} to 83.3 kcal mol^{-1} upon merging with the phenyl acrylonitrile moiety.

Along these lines, when its *p*-OH derivative **24** is compared with benzothiazole **21**, it preserves a lower ionization energy of IE = 127.1 kcal mol^{-1}, which confirms its higher FRAP activity. Unlike in benzothiazole, the benzimidazole N–H site is prone to further substitution, which motivated us to inspect the effect of the alkyl and aryl substituents on this site. It turned out that regardless of placing either small methyl (**36**), larger branched isobutyl (**30**) or aromatic phenyl (**42**) moieties on the benzimidazole amine, the resulting ionization energies and $\Delta G_R(H^\bullet)$ values change only marginally.

One could, perhaps, argue that, for example, a slightly lower $\Delta G_R(H^\bullet)$ value in **36** is responsible for a fivefold increase in the ABTS activity over **30**, yet we can conclude that the substitution of the benzimidazole N–H unit generally does induce any significant improvement in the antioxidant activity, and should not be pursued any further. On the other hand, the cyano group attached to the benzimidazole core groups the ionization energies in **27**–**29** around 131 kcal mol^{-1}, yet it allows a successive decrease in the $\Delta G_R(H^\bullet)$ values with each –OH group placed on the phenyl core. This, with the fact that, among the three systems, the IE value for **28** is lowest at 130.2 kcal mol^{-1}, makes it the most potent antioxidant in this work, thereby again confirming the crucial role of the electron liberation for the measured antioxidant activities.

3. Conclusions

This study details the design, synthesis, computational analysis, and biological assessment of novel methoxy, hydroxy, and N-substituted benzazole derived acrylonitriles. The specific design aimed to investigate the impact of varying methoxy and hydroxy group quantities, along with the type of substituent positioned at the N atom of the benzimidazole core, on their biological activity. All compounds were synthesized using established and optimized organic synthesis methods previously developed within our research group.

These synthesized compounds underwent evaluation for their antiproliferative activity against diverse cancer types. A significant number of these compounds exhibited potent and selective antiproliferative effects against the pancreatic adenocarcinoma cell line Capan-1 (with IC_{50} values ranging from 1.2 to 5.3 μM). Consequently, they were further tested against additional types of pancreatic adenocarcinoma cells. Their efficacy in inhibiting the growth of pancreatic adenocarcinoma spheroids and their selectivity towards normal PBMC cells were also assessed. Notably, among all the derivatives tested, the monohydroxy-substituted benzimidazole derivative **27** emerged with the most profound and broad-spectrum anticancer antiproliferative activity. This compound lacked a substituent on the benzimidazole nitrogen but featured a cyano group at the C-5(6) position of the benzimidazole. Compound **27** demonstrated non-toxicity towards normal cells. Furthermore, the impact of compound **27** on the cell cycle distribution of Capan-1 cancer cells was investigated, revealing through high-content analysis that treatment with derivative **27** effectively induced apoptosis in Capan-1 cells in a dose-dependent manner. Moreover, derivative **27** notably reduced the clonogenic survival of pancreatic adenocarcinoma cells.

Moreover, all compounds underwent assessment for their antioxidative potential utilizing various established methods.

The majority of the tested compounds exhibited significant antioxidative activity, notably observed through the FRAP method, often surpassing the standard BHT (3200 – 5235 $mmolFe^{2+}/mmolC$).

Computational analysis demonstrated the crucial role of the electron ionization for the observed antioxidative activities and rationalized the usefulness of the benzimidazole core over benzothiazole for the design of potent antioxidants. It also revealed that systems dressed with hydroxy groups benefit from their electron-donating effect, which compensates some of the lost electron density induced by expelled electrons and lowers ionization energies. The latter surpasses the stabilizing effect of the trihydroxy derivatives through their ability to form the O–H···O•···H–O hydrogen bonding with the radical center following the H• abstraction, thus making the dihydroxy derivative **28** the most potent antioxidant investigated here.

To explore a possible correlation between antioxidant and antiproliferative activity, derivatives exhibiting significant biological activity (**25**, **27**, **28**, **31**, **32**, **34**, **37**, **40**, **43**, **44**, and **46**) underwent an assay evaluating hydrogen peroxide (H_2O_2)-induced hemolysis, commonly used for assessing antioxidant activity. However, regression analysis only revealed a weak correlation between antiproliferative and antioxidant activities, suggesting their lack of direct relationship. Therefore, further experiments are necessary to elucidate the underlying mechanism of action for their anticancer effects.

4. Experimental section

4.1. Chemistry

4.1.1. General methods

All chemicals and solvents used in the study were procured from commercial suppliers, Aldrich and Acros. Melting points were determined using an SMP11 Bibby apparatus. NMR spectra were acquired in DMSO-d6 solutions employing TMS as the internal standard. Both 1H and 13C NMR spectra were recorded using a Varian Bruker Avance III HD 400 MHz/54 mm Ascend instrument. Chemical shifts are expressed in ppm (δ) relative to TMS. The synthesis of acrylonitrile derivatives was conducted in a Radleys Carousel 12 Plus parallel synthesis reactor. Flash chromatography was performed on an Interchim PuriFlash® device utilizing commercially available columns (Interchim PF-15SIHC-JP/ 4 and 12 g) packed with spherical silica gel (particle size 15 μm). Compound validation was routinely conducted via TLC using Merck silica gel 60F-254 glass plates.

Elemental analysis for C, H, and N content was carried out using a Perkin-Elmer 2400 elemental analyzer. When represented solely by elemental symbols, the analytical results obtained were within 0.4% of the theoretical value.

4.1.2. General method for preparation of compounds 17–47

A solution of equimolar amounts of 2-benzothiazole-acetonitrile **1**, 2-cyanomethyl-benzmidazoles **2**–**9**, and corresponding methoxy and hydroxy-substituted aromatic aldehyde **10**–**16** and piperidine in absolute ethanol were refluxed for 2 h. After the reaction mixture was cooled to room temperature, the crude product was filtered and recrystallized from ethanol if needed. Compounds **17-23** were prepared from **1** (0.6 mmol) and **10**–**16** (0.6 mmol).

(E)-2-(benzo[d]thiazol-2-yl)-3-phenylacrylonitrile 17

17 was prepared in yield 0.10 g (68%) as light yellow powder. m.p 196–200 °C; ^{1}H NMR (600 MHz, DMSO-*d*$_6$): δ/ppm = 8.45 (s, 1H, H_{arom}), 8.20 (d, 1H, *J* = 7.99 Hz, H_{arom}), 8.13-8.08 (m, 3H, H_{arom}), 7.64-7.61 (m, 3H, H_{arom}), 7.61-7.58 (m, 1H, H_{arom}), 7.55-7.52 (m, 1H, H_{arom}); ^{13}C NMR (151 MHz, DMSO-*d*$_6$): δ/ppm = 168.4, 158.1, 153.6, 139.6, 137.6, 137.6, 135.4, 134.5, 132.4, 131.6, 128.4, 127.7, 121.3, 110.8; Anal. Calcd. for $C_{16}H_{10}N_2S$: C, 73.26; H, 3.84; N, 10.68. Found: C, 73.36; H, 3.78; N, 10.60%.

(E)-2-(benzo[d]thiazol-2-yl)-3-(2-methoxyphenyl)acrylonitrile 18

18 was prepared in yield 0.09 g (57%) as yellow powder. m.p 200–203 °C;
^{1}H NMR (300 MHz, DMSO-*d*$_6$): δ/ppm = 8.56 (s, 1H, H_{arom}), 8.17 (t, 3H, *J* = 7.45 Hz, H_{arom}), 8.10 (d, 2H, *J* = 8.06 Hz, H_{arom}), 7.66-7.61 (m, 1H, H_{arom}), 7.61-7.56 (m, 1H, H_{arom}), 7.55-7.49 (m, 1H, H_{arom}), 7.24 (d, 1H, *J* = 8.38 Hz, H_{arom}), 7.17 (t, 1H, *J* = 7.57 Hz, H_{arom}), 3.95 (s, 3H, OCH_3); ^{13}C NMR (151 MHz, DMSO-*d*$_6$): δ/ppm = 163.6, 158.9, 153.4, 142.8, 134.9, 134.7, 128.8, 127.7, 126.8, 123.6, 123.0, 121.3, 121.3, 116.6, 112.6, 105.8, 56.6; Anal. Calcd. for $C_{17}H_{12}N_2OS$: C, 69.84; H, 4.14; N, 9.58. Found: C, 69.89; H, 4.09; N, 9.63%.

(E)-2-(benzo[d]thiazol-2-yl)-3-(2,4-dimethoxyphenyl)acrylonitrile 19

19 was prepared in yield 0.16 g (88%) as yellow powder. m.p 203–205 °C; ^{1}H NMR (300 MHz, DMSO-*d*$_6$): δ/ppm = 8.48 (s, 1H, H_{arom}), 8.24 (d, 1H, *J* = 8.78 Hz, H_{arom}), 8.14 (d, 1H, *J* = 7.59 Hz, H_{arom}), 8.06 (d, 1H, *J* = 7.99 Hz, H_{arom}), 7.60-7.54 (m, 1H, H_{arom}), 7.51-7.45 (m, 1H, H_{arom}), 6.79 (dd, 1H, J_1 = 2.37 Hz, J_2 = 8.79 Hz, H_{arom}), 6.74 (d, 1H, *J* = 2.39 Hz, H_{arom}), 3.96 (s, 3H, OCH_3), 3.90 (s, 3H, OCH_3);
^{13}C NMR (151 MHz, DMSO-*d*$_6$): δ/ppm = 165.4, 164.3, 161.1, 153.5, 141.6, 134.4, 130.0, 127.5, 126.4, 123.3, 122.8, 117.4, 114.1, 107.5, 101.5, 98.9, 56.8, 56.4; Anal. Calcd. for $C_{18}H_{14}N_2O_2S$: C, 67.06; H, 4.38; N, 8.69. Found: C, 67.11; H, 4.25; N, 8.63%.

(E)-2-(benzo[d]thiazol-2-yl)-3-(3,4,5-trimethoxyphenyl)acrylonitrile 20

20 was prepared in yield 0.17 g (85%) as yellow powder. m.p 199–201 °C; ^{1}H NMR (600 MHz, DMSO-*d*$_6$): δ/ppm = 8.37 (s, 1H, H_{arom}), 8.19 (d, 1H, *J* = 7.50 Hz, H_{arom}), 8.08 (d, 1H, *J* = 7.86 Hz, H_{arom}), 7.61-7.58 (m, 1H, H_{arom}), 7.56 (s, 2H, H_{arom}), 7.54-7.51 (m, 1H, H_{arom}), 3.87 (s, 6H, OCH_3), 3.80 (s, 3H, OCH_3); ^{13}C NMR (151 MHz, DMSO-*d*$_6$): δ/ppm = 163.8, 153.4, 148.6, 141.7, 134.7, 127.9, 127.6, 126.7, 123.5, 122.9, 116.9, 108.6, 104.4, 60.8, 56.5; Anal. Calcd. for $C_{19}H_{16}N_2O_3S$: C, 64.76; H, 4.58; N, 7.95. Found: C, 64.84; H, 4.51; N, 7.90%.

(E)-2-(benzo[d]thiazol-2-yl)-3-(4-hydroxyphenyl)acrylonitrile 21

21 was prepared in yield 0.11 g (71%) as yellow powder. m.p 211–215 °C; ^{1}H NMR (300 MHz, DMSO-d_6): δ/ppm = 10.60 (s, 1H, OH), 8.27 (s, 1H, H_{arom}), 8.16 (d, 1H, J = 7.48 Hz, H_{arom}), 8.04 (d, 3H, J = 8.87 Hz, H_{arom}), 7.63-7.54 (m, 1H, H_{arom}), 7.53-7.45 (m, 1H, H_{arom}), 6.98 (d, 2H, J = 8.66 Hz, H_{arom}); ^{13}C NMR (151 MHz, DMSO-d_6): δ/ppm = 164.4, 162.5, 153.5, 148.5, 134.5, 133.6, 127.5, 126.4, 123.9, 123.3, 122.8, 117.4, 116.8, 100.9; Anal. Calcd. for $C_{16}H_{10}N_2OS$: C, 69.05; H, 3.62; N, 10.07. Found: C, 69.11; H, 3.56; N, 9.94%.

(E)-2-(benzo[d]thiazol-2-yl)-3-(3,4-dihydroxyphenyl)acrylonitrile 22

22 was prepared in yield 0.08 g (47%) as yellow powder. m.p 214–218 °C; ^{1}H NMR (400 MHz, DMSO-d_6,): δ/ppm = 8.10 (d, 1H, J = 7.79 Hz, H_{arom}), 8.04 (s, 1H, H_{arom}), 7.98 (d, 1H, J = 8.00 Hz, H_{arom}), 7.65 (d, 1H, J = 2.08 Hz, H_{arom}), 7.53 (t, 1H, J = 7.17 Hz, H_{arom}), 7.46-7.35 (m, 2H, H_{arom}), 6.74 (d, 1H, J = 8.37 Hz, H_{arom}), 4.41 (bs, 2H, OH); ^{13}C NMR (151 MHz, DMSO-d_6,): δ/ppm = 165.6, 153.8, 148.0, 147.4, 134.2, 129.2, 127.2, 125.5, 122.6, 122.5, 120.9, 118.6, 116.6, 113.4, 44.4; Anal. Calcd. for $C_{16}H_{10}N_2O_2S$: C, 65.29; H, 3.42; N, 9.52. Found: C, 65.36; H, 3.37; N, 9.60%.

(E)-2-(benzo[d]thiazol-2-yl)-3-(3,4,5-trihydroxyphenyl)acrylonitrile 23

23 was prepared in yield 0.11 g (64%) as yellow powder. m.p 212–215 °C; ^{1}H NMR (300 MHz, DMSO-d_6,): δ/ppm = 9.41 (bs, 2H, OH), 8.14 (d, 1H, J = 7.57 Hz, H_{arom}), 8.03 (d, 2H, J = 7.09 Hz, H_{arom}), 7.60-7.52 (m, 1H, H_{arom}), 7.50-7.44 (m, 1H, H_{arom}), 7.18 (s, 2H, H_{arom});
^{13}C NMR (151 MHz, DMSO-d_6,): δ/ppm = 164.7, 153.5, 149.1, 146.6, 140.2, 134.5, 127.4, 126.2, 123.2, 122.9, 122.7, 117.4, 110.9, 100.3; Anal. Calcd. for $C_{16}H_{10}N_2O_3S$: C, 61.93; H, 3.25; N, 9.03. Found: C, 61.87; H, 3.15; N, 9.12%.

(E)-2-(1H-benzo[d]imidazol-2-yl)-3-(4-hydroxyphenyl)acrylonitrile 24

24 was prepared from **2** (0.10 g, 0.6 mmol) and **14** (0.08 g, 0.6 mmol) in absolute ethanol (5 mL) after refluxing for 2 hours to yield 0.12 g (72%) of yellow powder. m.p 225–230 °C; ^{1}H NMR (600 MHz, DMSO-d_6,): δ/ppm = 12.93 (bs, 1H, $NH_{benzimidazole}$), 10.51 (bs, 1H, OH), 8.22 (s, 1H, H_{arom}), 7.95-7.90 (m, 2H, H_{arom}), 7.59 (bs, 2H, H_{arom}), 7.23 (d, 2H, J = 3.08 Hz, H_{arom}), 7.02-6.93 (m, 2H, H_{arom}); ^{13}C NMR (151 MHz, DMSO-d_6,): δ/ppm = 161.6, 148.6, 145.9, 132.6, 124.3, 117.4, 116.8, 98.1; Anal. Calcd. for $C_{16}H_{11}N_3O$: C, 73.55; H, 4.24; N, 16.08. Found: C, 73.61; H, 4.15; N, 16.12%.

(E)-2-(1H-benzo[d]imidazol-2-yl)-3-(3,4-dihydroxyphenyl)acrylonitrile 25

25 was prepared from **2** (0.10 g, 0.6 mmol) and **15** (0.09 g, 0.6 mmol) in absolute ethanol (5 mL) after refluxing for 2 hours to yield 0.10 g (55%) of yellow powder. m.p 228–231 °C; ^{1}H NMR (600 MHz, DMSO-d_6,): δ/ppm = 12.87 (s, 1H, $NH_{benzimidazole}$), 9.84 (s, 1H, OH), 8.12 (s, 1H,

H_{arom}), 7.65 (bs, 1H, H_{arom}), 7.59 (d, 1H, J = 2.18 Hz, H_{arom}), 7.53 (bs, 1H, H_{arom}), 7.33 (dd, 1H, J_1 = 2.17 Hz, J_2 = 8.37 Hz, H_{arom}), 7.23 (bs, 2H, H_{arom}), 6.93 (d, 1H, J = 8.28 Hz, H_{arom}); ^{13}C NMR (151 MHz, DMSO-d_6,): δ/ppm = 149.5, 147.7, 145.2, 145.1, 123.6, 123.6, 122.6, 121.4, 118.3, 116.3, 115.5, 115.2, 110.7, 96.6; Anal. Calcd. for $C_{16}H_{11}N_3O_2$: C, 69.31; H, 4.00; N, 15.15. Found: C, 69.39; H, 4.10; N, 15.12%.

(E)-2-(1H-benzo[d]imidazol-2-yl)-3-(3,4,5-trihydroxyphenyl)acrylonitrile 26

26 was prepared from **2** (0.10 g, 0.6 mmol) and **16** (0.10 g, 0.6 mmol) in absolute ethanol (5 mL) after refluxing for 2 hours to yield 0.10 g (56%) of yellow powder. m.p 222–225 °C; ^{1}H NMR (600 MHz, DMSO-d_6,): δ/ppm = 12.85 (bs, 1H, $NH_{benzimidazole}$), 9.41 (s, 2H, OH), 8.01 (s, 1H, Harom), 7.75-7.39 (m, 2H, Harom), 7.23 (d, 2H, J = 8.78 Hz, Harom), 7.08 (s, 2H, Harom); ^{13}C NMR (151 MHz, DMSO-d_6,): δ/ppm = 148.9, 146.6, 146.4, 143.9, 138.8, 135.2, 123.6, 123.5, 122.5, 119.4, 117.3, 111.7, 110.0, 97.6. Anal. Calcd. for $C_{16}H_{11}N_3O_3$: C, 65.53; H, 3.78; N, 14.33. Found: C, 65.47; H, 3.84; N, 14.22%.

(E)-2-(1-cyano-2-(4-hydroxyphenyl)vinyl)-1H-benzo[d]imidazole-5(6)-carbonitrile 27

27 was prepared from **6** (0.10 g, 0.5 mmol) and **14** (0.07 g, 0.5 mmol) in absolute ethanol (5 mL) after refluxing for 2 hours to yield 0.04 g (27%) of yellow powder. m.p 243–247 °C; ^{1}H NMR (600 MHz, DMSO-d_6,): δ/ppm = 8.29 (s, 1H, H_{arom}), 8.09 (d, 1H, J = 0.90 Hz, H_{arom}), 7.93 (d, 2H, J = 8.79 Hz, H_{arom}), 7.70 (d, 1H, J = 8.28 Hz, H_{arom}), 7.55 (dd, 1H, J_1 = 1.46 Hz, J_2 = 8.27 Hz, H_{arom}), 7.00-6.94 (m, 2H, H_{arom});

^{13}C NMR (151 MHz, DMSO-d_6,): δ/ppm = 162.1, 147.2, 132.9, 126.1, 124.1, 120.6, 117.4, 116.9, 104.2, 97.7; Anal. Calcd. for $C_{17}H_{10}N_4O$: C, 71.32; H, 3.52; N, 19.57. Found: C, 71.36; H, 3.57; N, 19.47%.

(E)-2-(1-cyano-2-(3,4-dihydroxyphenyl)vinyl)-1H-benzo[d]imidazole-5(6)-carbonitrile 28

28 was prepared from **6** (0.15 g, 0.8 mmol) and **15** (0.11 g, 0.8 mmol) in absolute ethanol (5 mL) after refluxing for 2 hours to yield 0.08 g (32%) of yellow powder. m.p 230–236 °C; ^{1}H NMR (600 MHz, DMSO-d_6,): δ/ppm = 10.67 (bs, 2H, OH), 8.20 (s, 1H, H_{arom}), 8.13 (s, 1H, H_{arom}), 7.73 (d, 1H, J = 8.27 Hz, H_{arom}), 7.64-7.59 (m, 2H, H_{arom}), 7.35 (dd, 1H, J_1 = 2.07 Hz, J_2 = 8.37 Hz, H_{arom}), 6.93 (d, 1H, J = 8.28 Hz, H_{arom}); ^{13}C NMR (151 MHz, DMSO-d_6,): δ/ppm = 163.9, 152.2, 151.5, 151.1, 147.9, 146.4, 126.5, 125.4, 124.3, 120.4, 117.2, 116.6, 116.2, 104.7, 96.4. Anal. Calcd. for $C_{17}H_{10}N_4O_2$: C, 67.55; H, 3.33; N, 18.53. Found: C, 67.51; H, 3.29; N, 18.48%.

(E)-2-(1-cyano-2-(3,4,5-trihydroxyphenyl)vinyl)-1H-benzo[d]imidazole-5(6)-carbonitrile 29

29 was prepared from **6** (0.10 g, 0.5 mmol) and **16** (0.08 g, 0.5 mmol) in absolute ethanol (3 mL) after refluxing for 2 hours to yield 0.09 g (48%) of yellow powder. m.p 213–216 °C; ^{1}H NMR (600 MHz, DMSO-d_6,): δ/ppm = 8.12 (s, 1H, H_{arom}), 7.72 (d, 1H, J = 8.29 Hz, H_{arom}), 7.60 (dd,

1H, J_1 = 1.45 Hz, J_2 = 8.30 Hz, H_{arom}), 7.10 (s, 2H, H_{arom}), 3.59 (s, 3H, OH); ^{13}C NMR (151 MHz, DMSO-d_6,): δ/ppm = 148.3, 146.6, 139.7, 126.5, 123.1, 120.4, 117.1, 110.3, 104.8, 96.5; Anal. Calcd. for $C_{17}H_{10}N_4O_3$: C, 64.15; H, 3.17; N, 17.60. Found: C, 64.23; H, 3.22; N, 17.55%.

(E)-3-(4-hydroxyphenyl)-2-(1-isobutyl-1H-benzo[d]imidazol-2-yl)acrylonitrile 30

30 was prepared from **3** (0.10 g, 0.5 mmol) and **14** (0.06 g, 0.5 mmol) in absolute ethanol (5 mL) after refluxing for 2 hours to yield 0.05 g (35%) of orange powder. m.p 242–246 °C;^{1}H NMR (600 MHz, DMSO-d_6,): δ/ppm = 8.11 (s, 1H, H_{arom}), 7.97-7.94 (m, 2H, H_{arom}), 7.69-7.66 (m, 2H, H_{arom}), 7.32-7.28 (m, 1H, H_{arom}), 7.26 (td, 1H, J_1 = 0.98 Hz, J_2 = 7.59 Hz, H_{arom}), 6.94-6.89 (m, 2H, H_{arom}), 4.32 (d, 2H, J = 7.50 Hz, CH_2), 2.21-2.12 (m, 1H, CH), 0.83 (d, 6H, J = 6.68 Hz, CH_3); ^{13}C NMR (151 MHz, DMSO-d_6,): δ/ppm = 162.8, 151.5, 148.1, 142.3, 136.8, 133.6, 133.0, 123.8, 123.4, 122.9, 119.6, 118.1, 117.2, 116.9, 111.8, 94.9, 51.2, 51.2, 29.6, 20.1; Anal. Calcd. for $C_{20}H_{19}N_3O$: C, 75.69; H, 6.03; N, 13.24. Found: C, 75.61; H, 5.97; N, 13.16%.

(E)-3-(3,4-dihydroxyphenyl)-2-(1-isobutyl-1H-benzo[d]imidazol-2-yl)acrylonitrile 31

31 was prepared from **3** (0.10 g, 0.5 mmol) and **15** (0.06 g, 0.5 mmol) in absolute ethanol (3 mL) after refluxing for 2 hours to yield 0.04 g (27%) of orange powder. m.p 236–240 °C; ^{1}H NMR (600 MHz, DMSO-d_6,): δ/ppm = 7.94 (s, 1H, H_{arom}), 7.64 (d, 2H, J = 8.80 Hz, H_{arom}), 7.61 (d, 1H, J = 2.26 Hz, H_{arom}), 7.30-7.22 (m, 3H, H_{arom}), 6.72 (d, 1H, J = 8.27 Hz, H_{arom}), 4.30 (d, 2H, J = 7.48 Hz, CH_2), 2.21-2.11 (m, 1H, CH), 0.83 (d, 6H, J = 6.63 Hz, CH_3);
^{13}C NMR (151 MHz, DMSO-d_6,): δ/ppm = 151.7, 150.9, 148.8, 146.9, 142.4, 136.8, 127.3, 126.9, 126.9, 124.0, 123.1, 122.7, 122.3, 119.3, 118.8, 116.2, 116.2, 116.1, 114.2, 111.7, 111.6, 51.2, 29.5, 20.1; Anal. Calcd. for $C_{20}H_{19}N_3O_2$: C, 72.05; H, 5.74; N, 12.60. Found: C, 72.11; H, 5.81; N, 12.54%.

(E)-2-(1-isobutyl-1H-benzo[d]imidazol-2-yl)-3-(3,4,5-trihydroxyphenyl)acrylonitrile 32

32 was prepared from **3** (0.10 g, 0.5 mmol) and **16** (0.07 g, 0.5 mmol) in absolute ethanol (3 mL) after refluxing for 2 hours to yield 0.03 g (20%) of orange powder. m.p 245–251 °C; ^{1}H NMR (600 MHz, DMSO-d_6,): δ/ppm = 9.46 (s, 1H, OH), 9.30 (s, 1H, OH), 7.89 (s, 1H, H_{arom}), 7.70-7.66 (m, 2H, H_{arom}), 7.33-7.29 (m, 1H, H_{arom}), 7.26 (td, 1H, J_1 = 1.03 Hz, J_2 = 7.62 Hz, H_{arom}), 7.10 (s, 2H, H_{arom}), 4.29 (d, 2H, J = 7.54 Hz, H_{arom}), 2.20-2.10 (m, 1H, CH), 0.83 (d, 6H, J = 6.67 Hz, CH_3); ^{13}C NMR (151 MHz, DMSO-d_6,): δ/ppm = 152.1, 148.2, 146.5, 142.3, 139.0, 136.7, 123.5, 123.5, 122.9, 119.6, 117.9, 111.8, 110.7, 110.2, 95.2, 51.27, 29.6, 20.1 (2C); Anal. Calcd. for $C_{20}H_{19}N_3O_3$: C, 68.75; H, 5.48; N, 12.03. Found: C, 68.68; H, 5.52; N, 12.10%.

(E)-2-(1-cyano-2-(4-hydroxyphenyl)vinyl)-1-isobutyl-1H-benzo[d]imidazole-6-carbonitrile 33

33 was prepared from **7** (0.08 g, 0.3 mmol) and **14** (0.04 g, 0.3 mmol) in absolute ethanol (3 mL) after refluxing for 2 hours to yield 0.04 g (34%) of orange powder. m.p 272–277 °C; ^{1}H NMR

(600 MHz, DMSO-d_6,): δ/ppm = 10.68 (bs, 1H, OH), 8.26 (d, 1H, J = 1.03 Hz, H_{arom}), 8.23 (s, 1H, H_{arom}), 8.02-7.97 (m, 2H, H_{arom}), 7.95 (d, 1H, J = 8.49 Hz, H_{arom}), 7.72 (dd, 1H, J_1 = 1.52 Hz, J_2 = 8.49 Hz, H_{arom}), 7.01-6.94 (m, 2H, H_{arom}), 4.39 (d, 2H, J = 7.57 Hz, CH_2), 2.19-2.12 (m, 1H, CH), 0.83 (d, 6H, J = 6.61 Hz, CH_3); ^{13}C NMR (151 MHz, DMSO-d_6,): δ/ppm = 162.3, 152.8, 150.7, 141.7, 139.7, 133.3, 126.7, 124.6, 124.1, 120.1, 117.6, 116.7, 113.4, 105.3, 94.6, 51.5, 29.7, 19.9; Anal. Calcd. for $C_{21}H_{18}N_4O$: C, 73.67; H, 5.30; N, 16.36. Found: C, 73.74; H, 5.22; N, 16.30%.

(E)-2-(1-cyano-2-(3,4-dihydroxyphenyl)vinyl)-1-isobutyl-1H-benzo[d]imidazole-6-carbonitrile 34

34 was prepared from **7** (0.10 g, 0.4 mmol) and **15** (0.06 g, 0.4 mmol) in absolute ethanol (3 mL) after refluxing for 2 hours to yield 0.04 g (25%) of yellow powder. m.p 281–284 °C; ^{1}H NMR (600 MHz, DMSO-d_6,): δ/ppm = 8.16 (s, 1H, H_{arom}), 8.01 (s, 1H, H_{arom}), 7.87 (d, 1H, J = 8.46 Hz, H_{arom}), 7.65 (dd, 1H, J_1 = 1.12 Hz, J_2 = 8.39 Hz, H_{arom}), 7.62 (d, 1H, J = 2.02 Hz, H_{arom}), 7.29 (dd, 1H, J_1 = 2.09 Hz, J_2 = 8.37 Hz, H_{arom}), 6.64 (d, 1H, J = 8.41 Hz, H_{arom}), 4.37 (d, 2H, J = 7.48 Hz, CH_2), 2.19-2.12 (m, 1H, CH), 0.83 (d, 6H, J = 6.63 Hz, CH_3); ^{13}C NMR (151 MHz, DMSO-d_6,): δ/ppm = 152.5, 152.0, 147.3, 141.9, 139.9, 128.5, 126.1, 123.9, 120.3, 118.9, 116.3, 113.4, 113.0, 104.9, 44.7, 29.6, 19.9 (2C); Anal. Calcd. for $C_{21}H_{18}N_4O_2$: C, 70.38; H, 5.06; N, 15.63. Found: C, 70.44; H, 5.12; N, 15.57%.

(E)-2-(1-cyano-2-(3,4,5-trihydroxyphenyl)vinyl)-1-isobutyl-1H-benzo[d]imidazole-6-carbonitrile 35

35 was prepared from **7** (0.08 g, 0.3 mmol) and **16** (0.05 g, 0.3 mmol) in absolute ethanol (3 mL) after refluxing for 2 hours to yield 0.08 g (61%) of yellow powder. m.p 276–280 °C; ^{1}H NMR (600 MHz, DMSO-d_6,): δ/ppm = 9.32 (bs, 2H, OH), 8.28-8.21 (m, 1H, H_{arom}), 7.99 (s, 1H, H_{arom}), 7.93 (d, 1H, J = 8.46 Hz, H_{arom}), 7.71 (dd, 1H, J_1 = 1.45 Hz, J_2 = 8.49 Hz, H_{arom}), 7.12 (s, 2H, H_{arom}), 4.37 (d, 2H, J = 7.50 Hz, CH_2), 2.18-2.10 (m, 1H, CH), 0.83 (d, 6H, J = 6.60 Hz, CH_3); ^{13}C NMR (151 MHz, DMSO-d_6,): δ/ppm = 153.3, 151.0, 146.5, 146.4, 141.7, 139.9, 139.7, 126.6, 125.4, 124.6, 123.1, 120.2, 117.6, 113.4, 110.5, 110.1, 105.2, 93.9, 51.5, 29.6, 19.9; Anal. Calcd. for $C_{21}H_{18}N_4O_3$: C, 67.37; H, 4.85; N, 14.96. Found: C, 67.44; H, 4.78; N, 14.88%.

(E)-3-(4-hydroxyphenyl)-2-(1-methyl-1H-benzo[d]imidazol-2-yl)acrylonitrile 36

36 was prepared from **4** (0.10 g, 0.6 mmol) and **14** (0.07 g, 0.6 mmol) in absolute ethanol (5 mL) after refluxing for 2 hours to yield 0.12 g (76%) of yellow powder. m.p 254–259 °C; ^{1}H NMR (600 MHz, DMSO-d_6,): δ/ppm = 10.52 (s, 1H, OH), 8.03 (s, 1H, H_{arom}), 8.00-7.93 (m, 2H, H_{arom}), 7.68 (dd, 1H, J_1 = 0.80 Hz, J_2 = 7.97 Hz, H_{arom}), 7.63 (d, 1H, J = 7.96 Hz, H_{arom}), 7.34-7.31 (m, 1H, H_{arom}), 7.30-7.25 (m, 1H, H_{arom}), 7.00-6.94 (m, 2H, H_{arom}), 3.97 (s, 3H, CH_3); ^{13}C NMR (151 MHz, DMSO-d_6,): δ/ppm = 161.8, 150.7, 148.6, 142.4, 137.1, 132.8, 124.3, 123.5, 122.9, 119.5,

117.9, 116.6, 111.2, 95.9, 32.1; Anal. Calcd. for $C_{17}H_{13}N_3O$: C, 74.17; H, 4.76; N, 15.26. Found: C, 74.23; H, 4.84; N, 15.32%.

(E)-3-(3,4-dihydroxyphenyl)-2-(1-methyl-1H-benzo[d]imidazol-2-yl)acrylonitrile 37

37 was prepared from **4** (0.10 g, 0.6 mmol) and **15** (0.08 g, 0.6 mmol) in absolute ethanol (5 mL) after refluxing for 2 hours to yield 0.10 g (62%) of yellow powder. m.p 255–260 °C; ^{1}H NMR (600 MHz, DMSO-d_6,): δ/ppm = 9.70 (bs, 1H, OH), 7.91 (s, 1H, H_{arom}), 7.67 (d, 1H, J = 7.88 Hz, H_{arom}), 7.64 (d, 1H, J = 2.20 Hz, H_{arom}), 7.63 (d, 1H, J = 7.98 Hz, H_{arom}), 7.38 (dd, 1H, J_1 = 2.17 Hz, J_2 = 8.45 Hz, H_{arom}), 7.34-7.30 (m, 1H, H_{arom}), 7.29-7.25 (m, 1H, H_{arom}), 6.91 (d, 1H, J = 8.27 Hz, H_{arom}), 3.96 (s, 3H, CH_3); ^{13}C NMR (151 MHz, DMSO-d_6,): δ/ppm = 151.1, 150.8, 148.8, 146.2, 142.4, 137.0, 125.1, 124.7, 123.5, 122.9, 119.5, 117.9, 116.4, 116.2, 111.1, 95.4, 32.0; Anal. Calcd. for $C_{17}H_{13}N_3O_2$: C, 70.09; H, 4.50; N, 14.42. Found: C, 70.13; H, 4.45; N, 14.36%.

(E)-2-(1-methyl-1H-benzo[d]imidazol-2-yl)-3-(3,4,5-trihydroxyphenyl)acrylonitrile 38

38 was prepared from **4** (0.10 g, 0.6 mmol) and **16** (0.09 g, 0.6 mmol) in absolute ethanol (5 mL) after refluxing for 2 hours to yield 0.14 g (80%) of yellow powder. m.p 246–251 °C; ^{1}H NMR (600 MHz, DMSO-d_6,): δ/ppm = 9.21 (bs, 2H, OH), 7.80 (s, 1H, H_{arom}), 7.67 (d, 1H, J = 7.90 Hz, H_{arom}), 7.62 (d, 1H, J = 7.95 Hz, H_{arom}), 7.34-7.30 (m, 1H, H_{arom}), 7.29-7.25 (m, 1H, H_{arom}), 7.12 (s, 2H, H_{arom}), 3.95 (s, 3H, CH_3);

^{13}C NMR (151 MHz, DMSO-d_6,): δ/ppm = 151.5, 148.9, 146.5, 142.4, 139.3, 137.0, 123.4, 123.3, 122.9, 119.5, 117.9, 111.1, 110.2, 95.1, 32.0; Anal. Calcd. for $C_{17}H_{13}N_3O_3$: C, 66.44; H, 4.26; N, 13.67. Found: C, 66.37; H, 4.31; N, 13.74%.

(E)-2-(1-cyano-2-(4-hydroxyphenyl)vinyl)-1-methyl-1H-benzo[d]imidazole-6-carbonitrile 39

39 was prepared from **8** (0.10 g, 0.5 mmol) and **14** (0.06 g, 0.5 mmol) in absolute ethanol (5 mL) after refluxing for 2 hours to yield 0.07 g (44%) of yellow powder. m.p 229–233 °C; ^{1}H NMR (600 MHz, DMSO-d_6,): δ/ppm = 8.26-8.22 (m, 1H, H_{arom}), 8.10 (s, 1H, H_{arom}), 8.01-7.98 (m, 2H, H_{arom}), 7.86 (d, 1H, J = 8.47 Hz, H_{arom}), 7.72 (dd, 1H, J_1 = 1.46 Hz, J_2 = 8.39 Hz, H_{arom}), 6.98-6.96 (m, 2H, H_{arom}), 4.02 (s, 3H, CH_3); ^{13}C NMR (151 MHz, DMSO-d_6,): δ/ppm = 161.2, 150.8, 150.3, 140.7, 138.8, 132.1, 125.6, 123.4, 123.0, 119.1, 116.6, 115.6, 111.7, 104.0, 94.0, 31.5; Anal. Calcd. for $C_{18}H_{12}N_4O$: C, 71.99; H, 4.03; N, 18.66. Found: C, 72.06; H, 4.11; N, 18.55%.

(E)-2-(1-cyano-2-(3,4-dihydroxyphenyl)vinyl)-1-methyl-1H-benzo[d]imidazole-6-carbonitrile 40

40 was prepared from **8** (0.10 g, 0.5 mmol) and **15** (0.07 g, 0.5 mmol) in absolute ethanol (5 mL) after refluxing for 2 hours to yield 0.10 g (60%) of yellow powder. m.p 210–215 °C; ^{1}H NMR (600 MHz, DMSO-d_6,): δ/ppm = 8.19 (s, 1H, J = 0.90 Hz, H_{arom}), 7.92 (s, 1H, H_{arom}), 7.82-7.80 (m, 1H, H_{arom}), 7.68 (dd, 1H, J_1 = 1.47 Hz, J_2 = 8.39 Hz, H_{arom}), 7.64 (d, 1H, J = 2.30 Hz, H_{arom}),

7.33 (dd, 1H, J_1 = 2.28 Hz, J_2 = 8.49 Hz, H_{arom}), 6.74 (d, 1H, J = 8.30 Hz, H_{arom}), 4.00 (s, 3H, CH_3); ^{13}C NMR (151 MHz, DMSO-d_6,): δ/ppm = 152.2, 152.1, 146.9, 141.9, 139.9, 127.0, 126.4, 124.1, 122.6, 120.3, 118.3, 116.3, 114.7, 112.6, 104.9, 32.5; Anal. Calcd. for $C_{18}H_{12}N_4O_2$: C, 68.35; H, 3.82; N, 17.71. Found: C, 68.27; H, 3.76; N, 17.79%.

(E)-2-(1-cyano-2-(3,4,5-trihydroxyphenyl)vinyl)-1-methyl-1H-benzo[d]imidazole-6-carbonitrile 41

41 was prepared from **8** (0.10 g, 0.5 mmol) and **16** (0.08 g, 0.5 mmol) in absolute ethanol (5 mL) after refluxing for 2 hours to yield 0.05 g (31%) of yellow powder. m.p 278–282 °C; ^1H NMR (600 MHz, DMSO-d_6,): δ/ppm = 8.24-8.20 (m, 1H, H_{arom}), 7.87 (s, 1H, H_{arom}), 7.84 (d, 1H, J = 8.38 Hz, H_{arom}), 7.71 (dd, 1H, J_1 = 1.45 Hz, J_2 = 8.40 Hz, H_{arom}), 7.13 (s, 2H, H_{arom}), 4.00 (s, 3H, CH_3); ^{13}C NMR (151 MHz, DMSO-d_6,): δ/ppm = 152.5, 151.9, 146.5, 141.9, 139.9, 126.5, 124.2, 122.5, 120.3, 117.9, 112.7, 110.4, 104.9, 32.5; Anal. Calcd. for $C_{18}H_{12}N_4O_3$: C, 65.06; H, 3.64; N, 16.86. Found: C, 65.17; H, 3.58; N, 16.77%.

(E)-3-(4-hydroxyphenyl)-2-(1-phenyl-1H-benzo[d]imidazol-2-yl)acrylonitrile 42

42 was prepared from **5** (0.10 g, 0.4 mmol) and **14** (0.05 g, 0.4 mmol) in absolute ethanol (3 mL) after refluxing for 2 hours to yield 0.12 g (86%) of yellow powder. m.p 257–260 °C; ^1H NMR (600 MHz, DMSO-d_6,): δ/ppm = 10.51 (bs, 1H, OH), 7.81-7.77 (m, 2H, H_{arom}), 7.75-7.72 (m, 2H, H_{arom}), 7.68-7.63 (m, 2H, H_{arom}), 7.62-7-59 (m, 3H, H_{arom}), 7.37-7.33 (m, 1H, H_{arom}), 7.32-7.29 (m, 1H, H_{arom}), 7.20 (d, 1H, J = 7.82 Hz, H_{arom}), 6.89 (d, 2H, J = 8.78 Hz, H_{arom}); ^{13}C NMR (151 MHz, DMSO-d_6,): δ/ppm = 161.9, 150.7, 147.9, 142.5, 137.4, 135.8, 132.7, 130.7, 129.9, 127.9, 124.4, 124.1, 123.7, 119.8, 116.7, 116.6, 110.9, 96.0; Anal. Calcd. for $C_{22}H_{15}N_3O$: C, 78.32; H, 4.48; N, 12.46. Found: C, 78.41; H, 4.54; N, 12.56%.

(E)-3-(3,4-dihydroxyphenyl)-2-(1-phenyl-1H-benzo[d]imidazol-2-yl)acrylonitrile 43

43 was prepared from **5** (0.10 g, 0.4 mmol) and **15** (0.06 g, 0.4 mmol) in absolute ethanol (3 mL) after refluxing for 2 hours to yield 0.02 g (16%) of yellow powder. m.p 248–253 °C; ^1H NMR (600 MHz, DMSO-d_6,): δ/ppm = 7.77 (d, 1H, J = 7.90 Hz, H_{arom}), 7.68-7.64 (m, 2H, H_{arom}), 7.62-7.57 (m, 4H, H_{arom}), 7.39 (d, 1H, J = 2.23 Hz, H_{arom}), 7.34-7.31 (m, 1H, H_{arom}), 7.29-7.26 (m, 1H, H_{arom}), 7.17 (d, 1H, J = 7.89 Hz, H_{arom}), 7.06 (dd, 1H, J_1 = 2.19 Hz, J_2 = 8.46 Hz, H_{arom}), 6.73 (d, 1H, J = 8.29 Hz, H_{arom}), 4.56 (bs, 2H, OH); ^{13}C NMR (151 MHz, DMSO-d_6,): δ/ppm = 152.3, 149.8, 147.4, 145.5, 141.5, 136.3, 134.9, 129.5, 128.7, 126.9, 124.8, 123.1, 122.5, 121.9, 118.6, 116.1, 115.1, 113.9, 109.7, 92.6; Anal. Calcd. for $C_{22}H_{15}N_3O_2$: C, 74.78; H, 4.28; N, 11.89. Found: C, 74.84; H, 4.16; N, 11.79%.

(E)-2-(1-phenyl-1H-benzo[d]imidazol-2-yl)-3-(3,4,5-trihydroxyphenyl)acrylonitrile 44

44 was prepared from **5** (0.10 g, 0.4 mmol) and **16** (0.06 g, 0.4 mmol) in absolute ethanol (3 mL) after refluxing for 2 hours to yield 0.09 g (56%) of yellow powder. m.p 236–241 °C; ^{1}H NMR (600 MHz, DMSO-*d*$_6$,): δ/ppm = 7.78 (d, 1H, *J* = 7.78 Hz, H_{arom}), 7.68-7.64 (m, 2H, H_{arom}), 7.63-7.57 (m, 3H, H_{arom}), 7.47 (s, 1H, H_{arom}), 7.36-7.32 (m, 1H, H_{arom}), 7.31-7.27 (m, 1H, H_{arom}), 7.18 (d, 1H, *J* = 7.90 Hz, H_{arom}), 6.85 (s, 2H, H_{arom}); ^{13}C NMR (151 MHz, DMSO-*d*$_6$,): δ/ppm = 151.2, 148.2, 146.5, 142.5, 139.4, 137.4, 135.9, 130.6, 129.8, 127.9, 124.3, 123.6, 123.0, 119.8, 116.9, 110.9, 109.9, 95.4; Anal. Calcd. for $C_{22}H_{15}N_3O_3$: C, 71.54; H, 4.09; N, 11.38. Found: C, 71.47; H, 4.16; N, 11.29%.

(E)-2-(1-cyano-2-(4-hydroxyphenyl)vinyl)-1-phenyl-1H-benzo[d]imidazole-6-carbonitrile 45

45 was prepared from **9** (0.10 g, 0.4 mmol) and **14** (0.05 g, 0.4 mmol) in absolute ethanol (3 mL) after refluxing for 2 hours to yield 0.10 g (74%) of yellow powder. m.p 239–243 °C; ^{1}H NMR (600 MHz, DMSO-*d*$_6$,): δ/ppm = 10.56 (bs, 1H, OH), 8.37 (d, 1H, *J* = 1.04 Hz, H_{arom}), 7.85 (s, 1H, H_{arom}), 7.75 (d, 2H, *J* = 8.79 Hz, H_{arom}), 7.70-7.62 (m, 6H, H_{arom}), 7.34 (d, 1H, *J* = 8.49 Hz, H_{arom}), 6.90 (d, 2H, *J* = 8.80 Hz, H_{arom}); ^{13}C NMR (151 MHz, DMSO-*d*$_6$,): δ/ppm = 162.3, 151.9, 150.7, 142.0, 140.1, 135.0, 133.0, 130.7, 130.4, 128.1, 127.6, 124.7, 123.8, 120.0, 116.7, 116.4, 112.5, 105.9, 95.1; Anal. Calcd. for $C_{23}H_{14}N_4O$: C, 76.23; H, 3.89; N, 15.46. Found: C, 76.31; H, 3.93; N, 15.40%.

(E)-2-(1-cyano-2-(3,4-dihydroxyphenyl)vinyl)-1-phenyl-1H-benzo[d]imidazole-6-carbonitrile 46

46 was prepared from **9** (0.08 g, 0.3 mmol) and **15** (0.04 g, 0.3 mmol) in absolute ethanol (3 mL) after refluxing for 2 hours to yield 0.07 g (63%) of yellow powder. m.p 246–250 °C; ^{1}H NMR (600 MHz, DMSO-*d*$_6$,): δ/ppm = 8.39-8.36 (m, 1H, H_{arom}), 7.70-7.64 (m, 8H, H_{arom}), 7.42 (d, 1H, *J* = 2.21 Hz, H_{arom}), 7.34-7.31 (m, 1H, H_{arom}), 7.12 (dd, 1H, J_1 = 2.17 Hz, J_2 = 8.58 Hz, H_{arom}), 6.84 (d, 1H, *J* = 8.26 Hz, H_{arom}); ^{13}C NMR (151 MHz, DMSO-*d*$_6$,): δ/ppm = 151.0, 150.4, 149.8, 145.1, 140.9, 139.0, 134.0, 129.7, 129.3, 126.9, 126.5, 124.4, 123.6, 123.0, 118.9, 115.4, 115.3, 114.9, 111.4, 104.8, 93.5; Anal. Calcd. for $C_{23}H_{14}N_4O_2$: C, 73.01; H, 3.73; N, 14.81. Found: C, 73.12; H, 3.78; N, 14.75%.

(E)-2-(1-cyano-2-(3,4,5-trihydroxyphenyl)vinyl)-1-phenyl-1H-benzo[d]imidazole-6-carbonitrile 47

47 was prepared from **9** (0.08 g, 0.3 mmol) and **16** (0.05 g, 0.3 mmol) in absolute ethanol (3 mL) after refluxing for 2 hours to yield 0.10 g (84%) of yellow powder. m.p 254–261 °C; ^{1}H NMR (600 MHz, DMSO-*d*$_6$,): δ/ppm = 9.32 (bs, 2H, OH), 8.39-8.34 (m, 1H, H_{arom}), 7.70-7.63 (m, 7H, H_{arom}), 7.52 (s, 1H, H_{arom}), 7.33-7.31 (m, 1H, H_{arom}), 6.86 (s, 2H, H_{arom}); ^{13}C NMR (151 MHz,

DMSO-d_6,): δ/ppm = 152.4, 150.9, 146.5, 142.0, 140.1, 139.9, 135.2, 130.8, 130.4, 128.0, 127.6, 124.7, 122.8, 120.0, 116.5, 112.4, 110.3, 105.8, 94.6; Anal. Calcd. for $C_{23}H_{14}N_4O_3$: C, 70.05; H, 3.58; N, 14.21. Found: C, 70.12; H, 3.49; N, 14.16%.

4.2. Biological activity

4.2.1. 2D proliferation assays

Adherent cell lines (Capan-1, MIA Paca-2, Panc-1, PSN-1, HCT-116, LN-229, NCI-H460) were plated in 384-well tissue culture plates (Greiner) at densities ranging from 500 to 1500 cells per well. After an overnight incubation, the cells were treated with seven different concentrations of the test compounds, ranging from 100 to 0.006 µM. For suspension cell lines (DND-41, HL-60, K-562, Z-138), cells were seeded in 384-well culture plates at densities ranging from 2500 to 5500 cells per well, treated with the same concentration points of the test compounds, and then incubated for 72 hours. Following the incubation period, the CellTiter 96® AQueous One Solution Cell Proliferation Assay (MTS reagent, Promega) was utilized according to the manufacturer's instructions. Absorbance readings of the samples were measured at 490 nm using a SpectraMax Plus 384 (Molecular Devices). The obtained optical density (OD) values were used to calculate the 50% inhibitory concentration (IC50). The compounds were evaluated in two independent experiments.

4.2.2. 3D proliferation assays

Pancreatic adenocarcinoma cell lines (Capan-1, MIA Paca-2, Panc-1, PSN-1) were seeded into 384-well PrimeSurface® 3D Culture Spheroid ULA Plates (S-BIO) at a density ranging from 500 to 200 cells per well. Following centrifugation, the plates were incubated at 37°C and monitored using an IncuCyte® device (Essen BioScience Inc., Ann Arbor, MI, USA) for real-time imaging. Images were captured every 12 hours using brightfield and phase microscopy, with one field imaged per well at 10x magnification. Upon reaching an average diameter of 200 – 400 nm (day 3), the spheroids were treated with varying concentrations of the test compounds. After centrifugation, the plates were continually monitored for an additional 10 days. Cell growth was quantified based on the average size of the spheroids analyzed using the IncuCyte® image analysis software. The determined changes in cell growth were used to calculate the IC50 values. All compounds underwent testing in two independent experiments.

4.2.3. PBMC viability assay

Buffy coat preparations sourced from healthy donors were procured from the Blood Transfusion Center in Leuven, Belgium. Peripheral blood mononuclear cells (PBMC) were isolated using density gradient centrifugation over Lymphoprep (d=1.077 g/ml) (Nycomed, Oslo, Norway) and cultured in a cell culture medium (DMEM/F12, Gibco Life Technologies, USA) supplemented with 8% FBS. Freshly prepared PBMC were seeded at a density of 28,000 cells per well in 384-well culture plates containing various concentrations of the test compounds. The cells were then incubated for 72 hours with the compounds before analysis using the MTS reagent as per the manufacturer's instructions. The absorbance of the samples was measured at 490 nm using a SpectraMax Plus 384 (Molecular Devices). The obtained optical density (OD) values were used to determine the 50% inhibitory concentration (IC50). These compounds underwent testing in three independent experiments, with PBMC sourced from three distinct donors.

4.2.4. Antioxidative activity - erythrocyte hemolysis assay

Chicken blood collected in EDTA vials was centrifuged for 10 minutes at 1800 rpm to separate the supernatant and pellet. The pellet underwent two washes with PBS before being resuspended in a 2% PBS solution. Test and reference compounds were diluted in PBS and combined with the erythrocyte suspension. The mixtures were incubated at room temperature for 15 minutes. Subsequently, H2O2 solution was introduced to induce oxidative degradation of membrane lipids, incubating the samples for 2 hours at 37°C.

Following incubation, the samples were centrifuged at 1800 rpm for 10 minutes, and the absorbance of the supernatant was measured spectrophotometrically at 540 nm. The degree of hemolysis was determined relative to the hemolysis observed in the H2O2-treated negative control (PBS), which was set at 100%. The compounds underwent testing in two independent experiments.

4.2.5. Apoptosis induction

Capan-1 cells were plated at a density of 10,000 cells per well in 96-well, black-walled, clear-bottomed tissue culture plates. Following an overnight incubation, the cells were exposed to the test compounds at six varying concentrations spanning from 100 to 0.3 μM and were further incubated for 24 hours. Hoechst 33342 from BioRad and CellEvent TM Caspase-3/7 Green Detection reagent from Invitrogen were introduced according to the respective supplier instructions. Using high content image analysis (CellInsight CX5, ThermoFisher Scientific), fluorescence in the green channel was quantified, encompassing a minimum of 1000 cells per condition. The compounds underwent testing in two independent experiments.

4.2.6. Cell cycle

Capan-1 cells were initially seeded at a density of 10,000 cells per well in 96-well, black-walled, clear-bottomed tissue culture plates. Following an overnight incubation, the cells were exposed to the test compounds at six varying concentrations spanning from 100 to 0.3 µM, and further incubated for 24 hours. Subsequently, the cells underwent fixation with 4% PFA in PBS for 10 minutes, followed by washing and staining of the nuclei with DAPI. Plate imaging was conducted utilizing a CX5 High Content Screening device (ThermoFisher Scientific) employing the Cell Cycle Analysis bio-application, analyzing a minimum of 1000 cells per condition. The compounds were evaluated in two independent experiments.

4.2.7. Colony formation

The colony-forming capacity of pancreatic adenocarcinoma cell lines (Capan-1; Panc-1) was evaluated by initially seeding 500 cells onto 12-well plates. Following an overnight incubation, the growth medium was replaced with fresh medium supplemented with varying concentrations of AOH-011. The plates were then placed in an IncuCyte® device (Essen BioScience Inc., Ann Arbor, MI, USA) and incubated at 37°C. Real-time imaging was conducted over approximately 14 days to observe the growth of discernible colonies. Whole-well phase images were captured every 12 hours using 10x magnification. Cell growth was assessed as the percentage of confluence per well utilizing the IncuCyte® image analysis software.

To visualize the colonies, cells were fixed in 4% PFA in PBS for 20 minutes, washed with PBS, and subsequently stained with 1% crystal violet in 20% ethanol for an additional 20 minutes. Post-staining, the plates were rinsed with water and then scanned.

4.3. Antioxidative activity

Determination of the reducing activity of the stable radical 1,1-diphenyl-picrylhydrazyl (DPPH)

The assessment of the reducing activity of the studied systems was conducted using the DPPH method with adaptations to suit a 96-well microplate. In summary, equal volumes of different concentrations of the tested compounds (dissolved in DMSO) were mixed with a solution of DPPH (final concentration 50 µM in absolute ethanol). Control solutions comprising ethanol and DMSO were employed as references, consistent with previously reported methods.

Determination of Ferric Reducing/Antioxidant Power (FRAP assay)

The FRAP method was carried out according to previously described procedures with some modifications to be compatible with an assay on a 96-well microplate.

All results were expressed as Fe^{2+} equivalents (Fe^{2+} μmol). All tests were done in triplicate and the results were averaged and presented in Table 1.

ABTS Radical Scavenging Assay

The total antioxidant activity (TEAC) method was adapted for use with a microplate reader. Initially, the ABTS•+ (2,2′-azino-bis(3-ethylbenzothiazoline-6-sulfonic acid) radical cation) was generated by combining an ABTS stock solution (7 mM in water) with 2.45 mM potassium persulfate and allowed to stand for 12–16 hours at room temperature in darkness until it achieved a stable oxidative state. On the day of analysis, the ABTS•+ solution was diluted with PBS (pH 7.4) to attain an absorbance of 0.700 ± 0.01 at 734 nm. This radical state remained stable for over two days when stored in the dark at room temperature. Standards and solutions of the tested compounds (10 μL) were mixed with the working ABTS•+ solution (200 μL) in microplate wells and incubated at room temperature for 5 minutes. The reduction in absorbance at 734 nm was measured using a μQuant (Biotec Inc.) microplate reader. Aqueous phosphate buffer solution and Trolox (0.20–1.25 mmol/L) served as the control and primary calibration standard, respectively. The outcomes were expressed as an average of three independent measurements in trolox equivalents (mmol TEAC/mmolC).

4.4. Computational analysis

As a good compromise between accuracy and feasibility, all geometrical parameters were optimized with the B3LYP density functional theory (DFT) and the 6–31+G(d) basis set followed by the harmonic frequency calculations. Thermal corrections were extracted from the matching frequencies without scaling factors, while the obtained structures were confirmed as true minima by the absence of imaginary vibrational frequencies. In this way, all reported values correspond to differences in Gibbs free energies at a room temperature (298 K) and a normal pressure (1 atm). To account for the solvation effects, we included the SMD polarizable continuum model with all parameters corresponding to pure ethanol (ε = 24.852), in line with conducted experiments, yielding the (SMD)/B3LYP/6–31+G(d) model employed here. The choice of this computational setup was prompted by its success in modeling mechanisms of various antioxidants,[42,51,52] and in reproducing kinetic and thermodynamic parameters of a variety of organic[53,54] and enzymatic reactions.[55,56] All calculations were performed using the Gaussian 16 software.[57]

According to the literature, there are multiple mechanisms describing the antioxidative properties of molecules.[58] Here we evaluated the three most frequent, and usually thermodynamically most preferred antioxidant mechanisms, namely (i) hydrogen atom transfer (HAT), related with the capacity to transfer $H^{\bullet}$ to a free radical, (ii) proton transfer (PT), related

with the ability to transfer H^+, and (iii) single electron transfer (SET) related with ejecting an electron from the system. All these mechanisms are characterized by the Gibbs free energies (ΔG_R), calculated for the following processes:

$M{-}H \rightarrow M^{\bullet} + H^{\bullet}$ ($\Delta G_R(H^{\bullet})$ for HAT)

$M{-}H \rightarrow M^{+} + H^{+}$ ($\Delta G_R(H^{+})$ for PT)

$M \rightarrow M^{\bullet+} + e^{-}$ (IE for SET)

In all cases, lower Gibbs free energies denote a better antioxidant activity

5. Acknowledgments

We greatly appreciate the financial support of the Croatian Science Foundation under the projects IP-2018-02-4379 and IP–2020–02–8090. R.V. wishes to thank the Zagreb University Computing Centre (SRCE) for granting computational resources on the ISABELLA cluster. D.D. and L.P. are grateful for excellent technical assistance by J. Punjwani, Y. Smolders, N. Van Winkel and N. Willems.

6. Conflict of interests

The authors declare no conflict of interest.

7. References

[1] C. Mattiuzzi, G. Lippi, Current Cancer Epidemiology, J. Epidemiol. Glob. Health 9 (2019) 217-222. https://doi.org/10.2991/jegh.k.191008.001.

[2] Y.T. Lee, Y.J. Tan, C.E. Oon, Benzimidazole and its derivatives as cancer therapeutics: The potential role from traditional to precision medicine, Acta Pharm. Sin B. 13 (2023) 478-497. https://doi.org/10.1016/j.apsb.2022.09.010.

[3] J.-X. Hu, C.-F. Zhao, W.-B. Chen, Q.-C. Liu, Q.-W. Li, Y.-Y. Lin, F. Gao, Pancreatic cancer: A review of epidemiology, trend, and risk factors, World J. Gastroenterol. 27 (2021) 4298-4321. https://doi.org/10.3748/wjg.v27.i27.4298.

[4] P. Rawla, T. Sunkara, V. Gaduputi, Epidemiology of Pancreatic Cancer: Global Trends, Etiology and Risk Factors, World J. Oncol. 10 (2019) 10-27. https://doi.org/10.14740/wjon1166.

[5] A. Adamska, A. Domenichini, M. Falasca, Pancreatic Ductal Adenocarcinoma: Current and Evolving Therapies, Int. J. Mol. Sci. 18 (2017) 1338. https://doi.org/10.3390/ijms18071338.

[6] D. R. Principe, P. W. Underwood, M. Korc, J. G. Trevino, H. G. Munshi, A. Rana, The Current Treatment Paradigm for Pancreatic Ductal Adenocarcinoma and Barriers to Therapeutic Efficacy. Front. Oncol. 11 (2021) 688377. https://doi.org/10.3389/fonc.2021.688377.

[7] J. Sun, C. C. Russell, C. J. Scarlett, A. McCluskey, Small molecule inhibitors in pancreatic cancer. RSC Med. Chem. 11 (2020) 164-183. https://doi.org/10.1039/c9md00447eI.

[8] H. Jiang, S. Hegde, B. L. Knolhoff, Y. Zhu, J. M. Herndon, M. A. Meyer, T. M. Nywening, W. G. Hawkins, I. M. Shapiro, D. T. Weaver, J. A. Pachter, A. Wang-Gillam, D. G. DeNardo, Targeting focal adhesion kinase renders pancreatic cancers responsive to checkpoint immunotherapy. Nat. Med. 22 (2016) 851-860. https://doi.org/10.1038/nm.4123.

[9] D. Carbone, M. De Franco, C. Pecoraro, D. Bassani, M. Pavan, S. Cascioferro, B. Parrino, G. Cirrincione, S. Dall'Acqua, S. Moro, V. Gandin, P. Diana, Discovery of the 3-Amino-1,2,4-triazine-Based Library as Selective PDK1 Inhibitors with Therapeutic Potential in Highly Aggressive Pancreatic Ductal Adenocarcinoma. Int. J. Mol. Sci. 24 (2023), 3679. https://doi.org/10.3390/ijms24043679.

[10] L. Zhang, J. Li, L. Zong, X. Chen, K. Chen, Z. Jiang, L. Nan, X. Li, W. Li, T. Shan, Q. Ma, Z. Ma, Reactive Oxygen Species and Targeted Therapy for Pancreatic Cancer. Oxid. Med. Cell. Longev. 2016 (2016) 1-9. https://doi.org/10.1155/2016/1616781.

[11] L. Kumar, S. Kumar, K. Sandeep, S. K. S. Patel, Therapeutic Approaches in Pancreatic Cancer: Recent Updates, Biomedicines 11 (2023) 1611. https://doi.org/10.3390/biomedicines11061611.

[12] P. Storz, KRas, ROS and the initiation of pancreatic cancer. Small GTPases, 8 (2016), 38-42. https://doi.org/10.1080/21541248.2016.1192714.

[13] R. Huang, H. Chen, J. Liang, Y. Li, J. Yang, C. Luo, Y. Tang, Y. Ding, X. Liu, Q. Yuan, H. Yu, Y. Ye, W. Xu, X. Xie, Dual Role of Reactive Oxygen Species and their Application in Cancer Therapy, J. Cancer 12 (2021) 5543-5561. https://doi.org/10.7150/jca.54699.

[14] C.H. Chang, S. Pauklin, ROS and TGFβ: from pancreatic tumour growth to metastasis, J. Exp. Clin. Cancer Res. 40 (2021) 152. https://doi.org/10.1186/s13046-021-01960-4.

[15] P.D. Ray, B.W. Huang, Y. Tsuji, Reactive oxygen species (ROS) homeostasis and redox regulation in cellular signaling, Cell Signal. 24 (2012) 981-990. https://doi.org/10.1016/j.cellsig.2012.01.008.

[16] R. Singh, P.P. Manna, Reactive oxygen species in cancer progression and its role in therapeutics, Explor. Med. 3 (2022) 43-57. https://doi.org/10.37349/emed.2022.00073.

[17] J.C. Patterson, B.A. Joughin, B. van de Kooij, D.C. Lim, D.A. Lauffenburger, M.B. Yaffe, ROS and Oxidative Stress Are Elevated in Mitosis during Asynchronous Cell Cycle Progression and

Are Exacerbated by Mitotic Arrest, Cell Systems 8 (2019) 163-167. https://doi.org/10.1016/j.cels.2019.01.005.

[18] H. Nakamura, K. Takada, Reactive oxygen species in cancer: Current findings and future directions. Cancer Sci. 112 (2021) 3945-3952. https://doi.org/10.1111/cas.15068.

[19] Y. Wang, H. Qi, Y. Liu, C. Duan, X. Liu, T. Xia, D. Chen, H. Piao, H.-X. Liu, The double-edged roles of ROS in cancer prevention and therapy, Theranostics 11 (2021) 4839-4857. https://doi.org/10.7150/thno.56747.

[20] M. Cykowiak, V. Krajka-Kuźniak, Role of Nrf2 in Pancreatic Cancer, Antioxidants 11 (2022) 98. https://doi.org/10.3390/antiox11010098.

[21] X. Han, J. Li, T.M. Brasky, P. Xun, J. Stevens, E. White, M.D. Gammon, K. He, Antioxidant Intake and Pancreatic Cancer Risk: the Vitamins And Lifestyle (VITAL) Study, Cancer 119 (2013) 1314-1320. https://doi.org/10.1002/cncr.27936.

[22] P. Chaudhary, P. Janmeda, A. O. Docea, B. Yeskaliyeva, A. F. A. Razis, B. Modu, D. Calina, J. Sharifi-Rad, Oxidative stress, free radicals and antioxidants: potential crosstalk in the pathophysiology of human diseases, Front. Chem. 11 (2023) 1158198. https://doi.org/10.3389/fchem.2023.1158198.

[23] N. Abdel Hadi, G. Reyes-Castellanos, A. Carrier, Targeting Redox Metabolism inPancreatic Cancer. Int. J.Mol. Sci. 22 (2021) 1534. https://doi.org/10.3390/ijms22041534.

[24] M. Valko, D. Leibfritz, J. Moncol, M.T.D. Cronin, M. Mazur, J. Telser, Free radicals and antioxidants in normal physiological functions and human disease, Int. J. Biochem. Cell Biol. 39 (2007) 44-84. https://doi.org/10.1016/j.biocel.2006.07.001.

[25] N. Durand, P. Storz, Targeting reactive oxygen species in development and progression of pancreatic cancer, Expert Rev. Anticancer Ther. 17 (2017) 19-31. https://doi.org/10.1080/14737140.2017.1261017.

[26] L. Zhang, J. Li, L. Zong, X. Chen, K. Chen, Z. Jiang, L. Nan, X. Li, W. Li, T. Shan, Q. Ma, Z. Ma, Reactive Oxygen Species and Targeted Therapy for Pancreatic Cancer. Oxid. Med. Cell. Longev. 2016 (2016) 1616781. https://doi.org/10.1155/2016/1616781.

[27] A. Thyagarajan, A.S. Forino, R.L. Konger, R.P. Sahu, Dietary Polyphenols in Cancer Chemoprevention: Implications in Pancreatic Cancer, Antioxidants 9 (2020) 651. https://doi.org/10.3390/antiox9080651.

[28] X.J. Wang, J.Y. Chen, L.Q. Fu, M.J. Yan, Recent advances in natural therapeutic approaches for the treatment of cancer, J. Chemother. 32 (2020) 53-65. https://doi.org/10.1080/1120009X.2019.1707417.

[29] J. Chen, J. Yang, L. Ma, J. Li, N. Shahzad, C.K. Kim, Structure-antioxidant activity relationship of methoxy, phenolic hydroxyl, and carboxylic acid groups of phenolic acids, Sci. Rep. 10 (2020) 2611. https://doi.org/10.1038/s41598-020-59451-z.

[30] J.S. Wright, E.R. Johnson, G.A. DiLabio, Predicting the Activity of Phenolic Antioxidants: Theoretical Method, Analysis of Substituent Effects, and Application to Major Families of Antioxidants, J. Am. Chem. Soc. 123 (2001), 1173-1183. https://doi.org/10.1021/ja002455u.

[31] L. Racané, M. Cindrić, N. Perin, P. Roškarić, K. Starčević, T. Mašek, M. Maurić, J. Dogan, G. Karminski-Zamola, Croat. Chem. Acta 90 (2017) 187-195. https://doi.org/10.5562/cca3146.

[32] M. Cindrić, I. Sović, M. Mioč, L. Hok, I. Boček, P. Roškarić, K. Butković, I. Martin-Kleiner, K. Starčević, R. Vianello, M. Kralj, M. Hranjec, Experimental and Computational Study of the Antioxidative Potential of Novel Nitro and Amino Substituted Benzimidazole/Benzothiazole-2-Carboxamides with Antiproliferative Activity, Antioxidants 8 (2019) 477. https://doi.org/10.3390/antiox8100477.

[33] I. Sović, M. Cindrić, N. Perin, I. Boček, I. Novakovic, A. Damjanović, T. Stanojković, M. Zlatović, M. Hranjec, B. Bertoša, Biological potential of novel methoxy and hydroxy substituted heteroaromatic amides designed as promising antioxidative agents: Synthesis, 3D-QSAR analysis and biological activity, Chem. Res. Toxicol. 32 (2019) 1880-1892. https://doi.org/10.1021/acs.chemrestox.9b00256.

[34] M. Parcheta, R. Świsłocka, S. Orzechowska, M. Akimowicz, R. Choińska, W. Lewandowski, Recent Developments in Effective Antioxidants: The Structure and Antioxidant Properties, Materials 14 (2021) 1984. https://doi.org/10.3390/ma14081984.

[35] M. Percino, M. Cerón, O. Rodríguez, G. Soriano-Moro, M. Castro, V. Chapela, M.A. Siegler, E. Pérez-Gutiérrez, Conformational and Molecular Structures of α,β-Unsaturated Acrylonitrile Derivatives: Photophysical Properties and Their Frontier Orbitals, Molecules 21 (2016) 389. https://doi.org/10.3390/molecules21040389.

[36] M.M. Sirim, V.S. Krishna, D. Sriram, O. Unsal Tan, Novel benzimidazole-acrylonitrile hybrids and their derivatives: Design, synthesis and antimycobacterial activity, Eur. J. Med. Chem. 15 (2020) 112010. https://doi.org/10.1016/j.ejmech.2019.112010.

[37] I. Briguglio, E. Laurini, M.A. Pirisi, S. Piras, P. Corona, M. Fermeglia, S. Pricl, A. Carta, Triazolopyridinyl-acrylonitrile derivatives as antimicrotubule agents: Synthesis, in vitro and in silico characterization of antiproliferative activity, inhibition of tubulin polymerization and binding thermodynamics, Eur. J. Med. Chem. 141 (2017) 460-472. http://doi.org/10.1016/j.ejmech.2017.09.065.

[38] S.S. AlNeyadi, A.A. Salem, M.A. Ghattas, N. Atatreh, I.M. Abdou, Antibacterial activity and mechanism of action of the benzazole acrylonitrile-based compounds: In vitro , spectroscopic, and docking studies, Eur. J. Med. Chem. 136 (2017) 270-282. https://doi.org/10.1016/j.ejmech.2017.05.010.

[39] C.J. Bethencourt-Estrella, S. Delgado-Hernández, A. López-Arencibia, D. San Nicolás-Hernández, D. Tejedor, F. Garciá-Tellado, J. Lorenzo-Morales, J.E. Piñero, *In vitro* activity and cell death mechanism induced by acrylonitrile derivatives against *Leishmania amazonensis*, Bioorg. Chem. 124 (2022) 105872. https://doi.org/10.1016/j.bioorg.2022.105872.

[40] F. Riu, R. Ibba, S. Zoroddu, S. Sestito, M. Lai, S. Piras, L. Sanna, V. Bordoni, L. Bagella, A. Carta, Design, synthesis, and biological screening of a series of 4'-fluoro-benzotriazole-acrylonitrile derivatives as microtubule-destabilising agents (MDAs), J. Enzyme Inhib. Med. Chem. 37 (2022) 2223-2240. https://doi.org/10.1080/14756366.2022.2111680.

[41] A. Konrnicka, K. Gzella, K. Garbacz, M. Jarosiewicz, M. Gdaniec, J. Fedorowicz, L. Balewski, J. Kokoszka, A. Ordyszewska, Indole-Acrylonitrile Derivatives as Potential Antitumor and Antimicrobial Agents-Synthesis, In Vitro and In Silico Studies, Pharmaceuticals 16 (2023) 918. https://doi.org/10.3390/ph16070918.

[42] N. Perin, L. Hok, A. Beč, L. Persoons, E. Vanstreels, D. Daelemans, M. Hranjec, N-substituted benzimidazole acrylonitriles as in vitro tubulin polymerization inhibitors: synthesis, biological activity and computational analysis, Eur. J. Med. Chem. 5 (2021) 113003. https://doi.org/10.1016/j.ejmech.2020.113003.

[43] A. Beč, L. Hok, L. Persoons, E. Vanstreels, D. Daelemans, R. Vianello, M. Hranjec, Synthesis, Computational Analysis, and Antiproliferative Activity of Novel Benzimidazole Acrylonitriles as Tubulin Polymerization Inhibitors: Part 2, Pharmaceuticals 14 (2021) 1052. https://doi.org/ 10.3390/ph14101052.

[44] C. Pecoraro, M. De Franco, D. Carbone, D. Bassani, M. Pavan, S. Cascioferro, B. Parrino, G. Cirrincione, S. Dall'Acqua, S. Moro, V. Gandin, P. Diana, 1,2,4-Amino-triazine derivatives as pyruvate dehydrogenase kinase inhibitors: Synthesis and pharmacological evaluation. Eur. J. Med. Chem. 249 (2023) 115134. https://doi.org/10.1016/j.ejmech.2023.115134.

[45] P. Nayak, V. Bentivoglio, M. Varani, A. Signore, Three-Dimensional In Vitro Tumor Spheroid Models for Evaluation of Anticancer Therapy: Recent Updates. Cancers 15(19) (2023) 4846. https://doi.org/10.3390/cancers15194846.

[46] G. Li Petri, C. Pecoraro, O. Randazzo, et al. New Imidazo[2,1-b][1,3,4]Thiadiazole Derivatives Inhibit FAK Phosphorylation and Potentiate the Antiproliferative Effects of Gemcitabine Through Modulation of the Human Equilibrative Nucleoside Transporter-1 in Peritoneal Mesothelioma. Anticancer Res. 40(9) (2020) 4913-4919. doi:10.21873/anticanres.14494.

[47] L. M. Mukherje, On the Determination of Autoprotolysis Constant of Ethanol J. Phys. Chem. 60 (1956) 1019-1020. https://doi.org/10.1021/j150541a053.

[48] S. Tshepelevitsh, A. Kütt, M. Lõkov, I. Kaljurand, J. Saame, A. Heering, P. Plieger, R. Vianello, I. Leito, Eur. J. Org.Chem. (2019) 6735-6748. https://doi.org/10.1002/ejoc.201900956.

[49] A. Beč, L. Racane, L. Žonja, L. Persoons, D. Daelemans, K. Starčević, R. Vianello, M. Hranjec, Biological evaluation of novel amidino substituted coumarin-benzazole hybrids as promising therapeutic agents, RSC Med. Chem. 14 (2023) 957-968. https://doi.org/10.1039/D3MD00055A.

[50] J. Chen, J. Yang, L. Ma, J. Li, N. Shahzad, C.K. Kim, Structure-antioxidant activity relationship of methoxy, phenolic hydroxyl, and carboxylic acid groups of phenolic acids, Sci. Rep. 10 (2020) 2611. https://doi.org/10.1038/s41598-020-59451-z.

[51] I. Boček, K. Starčević, I. Novak Jovanović, R. Vianello, M. Hranjec, Novel imidazo[4,5-b]pyridine derived acrylonitriles: A combined experimental and computational study of their antioxidative potential, J. Mol. Liq. 342 (2021) 117527. https://doi.org/10.1016/j.molliq.2021.117527.

[52] M. Cindrić, I. Sović, M. Mioč, L. Hok, I. Boček, P. Roškarić, K. Butković, I. Martin-Kleiner, K. Starčević, R. Vianello, M. Kralj, M. Hranjec, Experimental and Computational Study of the Antioxidative Potential of Novel Nitro and Amino Substituted Benzimidazole/Benzothiazole-2-Carboxamides with Antiproliferative Activity, Antioxidants 8 (2019) 477. https://doi.org/10.3390/antiox8100477.

[53] M. Toma, L. Božičević, J. Lapić, S. Đaković, D. Šakić, T. Tandarić, R. Vianello, V. Vrček, Transacylation in Ferrocenoyl- Purines. NMR and Computational Study of the Isomerization Mechanism, J. Org. Chem. 84 (2019) 12471-12480. https://doi.org/10.1021/acs.joc.9b01944.

[54] A. Alizadeh, A. Bagherinejad, J. Kayanian, R. Vianello, An experimental and computational study of new spiro-barbituric acid pyrazoline scaffolds: restricted rotation vs. annular tautomerism, New J. Chem. 46 (2022) 7242-7252. https://doi.org/10.1039/D1NJ06208E.

[55] E. Mehić, L. Hok, Q. Wang, I. Dokli, M. Svetec Miklenić, Z. Findrik Blažević, L. Tang, R. Vianello, M. Majerić Elenkov, Front Cover Picture: Expanding the Scope of Enantioselective Halohydrin Dehalogenases – Group B, Adv. Synth. Catal. 364 (2022) 2576-2588. https://doi.org/10.1002/adsc.202200342.

[56] T. Tandarić, R. Vianello, Computational Insight into the Mechanism of the Irreversible Inhibition of Monoamine Oxidase Enzymes by the Antiparkinsonian Propargylamine Inhibitors Rasagiline and Selegiline, ACS Chem. Neurosci. 10 (2019) 3532-3542. https://doi.org/10.1021/acschemneuro.9b00147.

[57] Gaussian 16, Revision C.01, M.J. Frisch, G.W. Trucks, H.B. Schlegel, G.E. Scuseria, M.A. Robb, J.R. Cheeseman, G. Scalmani, V. Barone, G.A. Petersson, H. Nakatsuji, X. Li, M. Caricato, A.V. Marenich, J. Bloino, B.G. Janesko, R. Gomperts, B. Mennucci, H.P. Hratchian, J.V. Ortiz, A.F. Izmaylov, J.L. Sonnenberg, D. Williams-Young, F. Ding, F. Lipparini, F. Egidi, J. Goings, B. Peng, A. Petrone, T. Henderson, D. Ranasinghe, V.G. Zakrzewski, J. Gao, N. Rega, G. Zheng, W. Liang, M. Hada, M. Ehara, K. Toyota, R. Fukuda, J. Hasegawa, M. Ishida, T. Nakajima, Y. Honda, O. Kitao, H. Nakai, T. Vreven, K. Throssell, J. A. Montgomery, Jr., J.E. Peralta, F. Ogliaro, M.J. Bearpark, J.J. Heyd, E.N. Brothers, K.N. Kudin, V.N. Staroverov, T.A. Keith, R. Kobayashi, J. Normand, K. Raghavachari, A.P. Rendell, J.C. Burant, S.S. Iyengar, J. Tomasi, M. Cossi, J.M. Millam, M. Klene, C. Adamo, R. Cammi, J.W. Ochterski, R.L. Martin, K. Morokuma, O. Farkas, J.B. Foresman, D.J. Fox, Gaussian, Inc., Wallingford CT, 2016.

[58] D. Huang, O.U. Boxin, R.L. Prior, The Chemistry behind Antioxidant Capacity Assays, J. Agric. Food Chem. 53 (2005) 1841-1856. https://doi.org/10.1021/jf030723c.